CAPITAL UNIVERSITY OF SCIENCE AND
TECHNOLOGY, ISLAMABAD

Watermarking of Segments of Brain MRI Produced by ANN

by

Mehwish Riaz

A thesis submitted in partial fulfillment for the
degree of Master of Science

in the

Faculty of Computing
Department of Computer Science

2022

My work is dedicated, firstly to the Almighty Allah, for blessing me with the opportunities, health and abilities to be where I am do what I did. After Allah, this study is wholeheartedly dedicated to my beloved parents, who have been my biggest inspiration, and specially to my support system, my father, for his constant moral, spiritual, emotional, and financial support.

CERTIFICATE OF APPROVAL

Watermarking of Segments of Brain MRI Produce by ANN with Different Noise and INU Level

by

Mehwish Riaz

(MCS191002)

THESIS EXAMINING COMMITTEE

S. No.	Examiner	Name	Organization
(a)	External Examiner	Dr. Muhammad Nazir	HITEC, Taxila
(b)	Internal Examiner	Dr. Abdul Basit Siddiqui	CUST, Islamabad
(c)	Supervisor	Dr. M. Masroor Ahmed	CUST, Islamabad

Dr. M. Masroor Ahmed
Thesis Supervisor
January, 2022

Dr. Nayyer Masood
Head
Dept. of Computer Science
January, 2022

Dr. M. Abdul Qadir
Dean
Faculty of Computing
January, 2022

Author's Declaration

I, **Mehwish Riaz** hereby state that my MS thesis titled "**Watermarking of Segments of Brain MRI Produced by ANN**" is my own work and has not been submitted previously by me for taking any degree from Capital University of Science and Technology, Islamabad or anywhere else in the country/abroad.

At any time if my statement is found to be incorrect even after my graduation, the University has the right to withdraw my MS Degree.

(Mehwish Riaz)
Registration No: MCS191002

Plagiarism Undertaking

I solemnly declare that research work presented in this thesis titled "**Watermarking of Segments of Brain MRI Produced by ANN**" is solely my research work with no significant contribution from any other person. Small contribution/help wherever taken has been duly acknowledged and that complete thesis has been written by me.

I understand the zero tolerance policy of the HEC and Capital University of Science and Technology towards plagiarism. Therefore, I as an author of the above titled thesis declare that no portion of my thesis has been plagiarized and any material used as reference is properly referred/cited.

I undertake that if I am found guilty of any formal plagiarism in the above titled thesis even after award of MS Degree, the University reserves the right to withdraw/revoke my MS degree and that HEC and the University have the right to publish my name on the HEC/University website on which names of students are placed who submitted plagiarized work.

(Mehwish Riaz)
Registration No: MCS191002

Acknowledgement

If you are grateful, **I would certainly give you more; and if you are ungrateful,My chastisement is truly severe.**(14:7) Alhamdulillah for everything Allah has blessed me with that helped me reach here. I would like to show my gratitude to my supervisor, who shared his words of advice and encouragement to this study and helped me through every difficulty regarding this study. I am thankful to my mother for pushing me for higher studies and my father for making everything I wish for possible for me. Lastly, I would like to thank my sister and my friends for always being there when I needed help and support

(Mehwish Riaz)

Abstract

One of the key requirements of a typical Electronic-Healthcare (E-Healthcare) system is the electronic transmission of medical images. This communication, however, could be vulnerable to hackers, who could alter the entire medical image or just a portion of it while in transit. Digital watermarking is used to ensure the integrity of medical images. As medical images carry different levels of complexities ,there is need to know which information should be watermarked so important information from medical image should be extracted through segmentation.This study used ANN based segmentation to extract region of interest from Brain MRI and then watermark those extracted segments by watermarking method based on discrete wave transformation , Hessenberg decomposition, and singular value decomposition.BrainWeb images with different Noise and INU level are used for this study.At first brain MRI's with 0,1 ,3 and 5 percent Noise and INU level are segmented into Gray matter (GM) ,Cerebrospinal fluid (CSF) and White matter (WM) then each segment is used as host image in watermarking process as the host images is first decomposed into a number of sub-bands using multilevel discrete wave transformation (DWT), and the resulting coefficients are then utilised as the input for Hessenberg decomposition (HD) in the embedding process. At the same time, the watermark is applied to the SVD. Invisibility and robustness of images is analyzed by calculating Peak signal-to-noise ratio (PSNR) , Structural Similarity Index (SSIM) and Normalized correlation (NC) values. proposed technique work well for all Noise and INU level and even for watermarks of various sizes, method achieves a reasonable balance of robustness and invisibility except for that watermark logo with size 128x128.

Contents

List of Figures

List of Tables

Abbreviations

ANN	Artificial Neural Network
BR	Bayesian Regularization
CT	Computed Tomography
CSF	Cerebrospinal Fluid
CSNN	Contextual Sentiment Neural Network
DCT	Discrete Cosine Transform
DWT	Discrete Wavelet Transform
EPR	Electronic Patient Record
FFNN	Feedforward Neural Network
GM	Gray Matter
HNN	Hopfield Neural Network
LMA	Levenberg Marquardt
MRI	Magnetic Resonance Imaging
PCNN	Pulse Coupled Neural Network
PET	Positron Emission Tomography
ROI	Region Of Interest
SCG	Scale Congugate Gradient
SVD	Singular Value Decomposition
SOMs	Self-Organizing Map
SPECT	Single Photon Emission Computed Tomography
WM	White Matter

Chapter 1

Introduction

1.1 Background

Medical imagery has been one of the most important techniques for the clinical diagnosis and treatment of human brain diseases in recent decades.X-raycomputedtomography ,positron-emission-tomography,single photon emission com-puted tomography ,and magnetic resonence imaging are just a few of the diagnostic imaging modalities that are quickly developing and widely employed to visualise anatomical features.

Medical images are a key and important aspect of medical knowledge because they have decisive properties.In One of the key requirements of a typical Electronic-Healthcare (E-Healthcare) system is the electronic transmission of medical images. This communication,however,could be vulnerable to hackers, who could alter the entire medical image or just a portion of it while in transit. Digital water-marking is used to ensure the integrity of medical images. As medical images carry different levels of complexities ,there is need to know which information should be water-marked so important information from medical image should be extracted t hrough segmentation.For ensuring intagrity of a medical-image,digital watermarking is important technique .

1.1.1 Techniques of Watermarking

Digital image watermarking can be characterised as spatial, transform, or hybrid domains depending on the working domain. The least significant bit (LSB), intermediate significant bit (ISB), and patchwork algorithms are examples of spatial domain approaches. DCT, DFT, DWT, and SVD are examples of transform or frequency domain methods. Two or more transform domain algorithms are combined in the hybrid domain approach. DCT and DFT, DCT and DWT, DCT and SVD, DFT and DWT, DFT and SVD, DWT and SVD, and a mix of DCT, DFT, and DWT and others are among them[1].Figure 1.1 shows some techniques of digital watermarking.

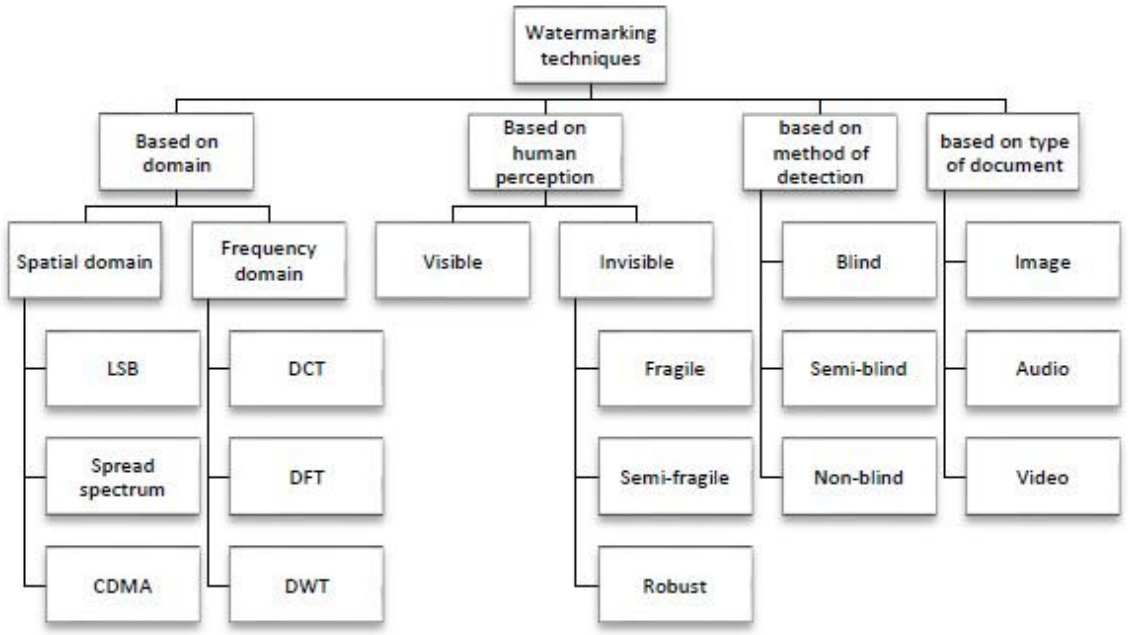

FIGURE 1.1: Techniques of watermarking [2]

1.1.2 Image Segmentation

In medical image processing, segmentation is very significant. To avoid ROI distortion in medical image analysis, the initial step is to segment the image. The process of partitioning an image into separate parts by grouping together neighbouring pixels based on some preset similarity criterion is known as image segmentation. Specific attributes of pixels in the image might be used to establish this

similarity criterion. In medical imaging, segmentation is utilised for extracting features, image presentation, and image measurement. Segmentation's purpose is to separate a whole medical image into subregions, i.e. (white and grey matter).This also aids in the classification of image pixels into anatomical regions (such as bones, muscles and blood vessels).

1.1.3 ANN Based Segmentation

ANN have become a popular technique for image segmentation. ANN-based segmentation algorithms have risen in popularity because to its proper-ties,which include a modest drop where noise is present, the ability to be used in realtime applications, and the implemented easily with Very large-scale integration procassors.Almost every sort of neural network has been used to varying degrees ofsuccess. Kohonen and Hopfield ANNs are the most commonly used. Feed-forward back-propagation neural, SOMs, HNN, CSNN neural networks are some of the techniques used (PCNN).

Related work in this domain is describe below

In the transform domain, the author[3] provides two distinct watermarking techniques for medical images. In the first technique, an watarmark and an EPR were added ROI and the RONI. For the diagnosis purpose, the ROI is left unal-tered, while the RONI is used to disguise the watermark and EPR in the second technique. Both techniques use an eight block DCT. DCT two coeffecients are chosen for embedding the watermark/ EPR, and their magnetudes are compared in 808 blocks. The coeffecients are then balanced by using a threshold of the wa-termark/EPR for adding 1 /0 bits. The results show that the proposed solutions are highly undetectable as well as resistant to many attack s such as sharpen-ing attack, Salt attack and Pepper noise attack, JPEG attacks, Gaussian noise attacks and rotation attacks, Cropping attacks, Filtering attacks, and so on. Pro-vide the effectiveness of strategies against a variety of threats. For colour images, the author[4] developeda cutting edge neural network-based digital watermark-ing approach. This metho embeds an watermark that is not visi-ble in

image and after that uses NN to successfully find out about the properties of the implanted watermark in relation to the image with a watermark. The authors [2] offer a fresh approach for watermarking based on NN and DCT. FCNN is the name of the neural network. The visual and perceptive features of the real image were simulated using FCNN. The greatest variable thrashold value s of DCT coeffecients were determined using perceptual properties of the real image. The watermark was added in DCT coeffecients of the real image using the greatest adjustable threshold values. A binary image is used as a watermark. In the DCT coefficients of this image, the values of pixel are introduced by 0 and 1. Results of the experiment reveal that method is sufficiently resilient against various types of watermarking attacks.

1.2 Motivation

Various work carried out in the domain of medical image watermarking but our motivation is to watermark brain MRI's with different level of complexities to achieves a reasonable balance of robustness and invisibility even for watermarks of various sizes.

1.3 Problem Statement

One of the key requirements of Electronic-Healthcare system is the transmission of medical imagess. Radiologists are needed to provide information for these medical images. It is difficult to transport images over a network due to their high s ize. This communication could also be vulnerable and hackers could alter the entire medical image or just a portion of it while in transit. A thorough review of the literature reveals various work carried out in this domain but still there is need to improve imperceptibility and robustness under different attacks. The goal of this study is to address this issue by developing the best ANN-based segmentation algorithm for dividing huge images into smaller chunks and then use suitable

watermarking technique on those segments with different noise level which will achieves a reasonable balance of robustness and invisibility even for watermarks of various sizes.

1.4 Research Problems

The above problem statement raises following research questions, which are stated below:

Q1: How we can default setting of ANN to precisely segment Brain MRI that hold different levels of Noise and INU?

Q2: Which technique will be used to watermark segments achieves a reasonable balance of robustness and invisibility under different attacks.

1.5 Research Methodology

The methodology of this research work is based on the experimental research method and it comprises of three main phases:

1. Exploratory
2. Implementation
3. Evaluation

1.5.1 Exploratory

This phase consists of a detailed study on the topic and review of the relevant literature found. This is done to identify the significance of the problem and find the shortcomings in already present solutions (if any).

1.5.2 Implementation

This phase is based on execution of the proposed solution. The proposed technique is implemented and compliance score of different documents is calculated.

1.5.3 Evaluation

The last phase of this research is the evaluation of the results computed from the proposed technique. The results computed from the proposed technique are analysed.

1.6 Thesis Organization

In Introduction chapter, a brief overview about the topic is given and the problem is explained. The significance of the problem and research methodology is also discussed. The chapter of Literature Review includes the findings of detailed literature survey that is performed to identify the implication of the problem. The content of chapter 2 answers the Research Question 1. The reviewed literature is discussed in detail and relevant information from the already existing literature is also added. The Chapter 3 presents the step-by-step solution of the problem.

A new technique is proposed that is expected to give best results as compared to techniques that are already being used, addressing the Research Question. The Chapter 4 discusses the final results calculate after implementation of the proposed solution show the performance of the proposed technique. These results are then evaluated in two steps, i.e., user-based testing and evaluation measures like precision, recall etc., thus solving the research question 3. The findings of this study are concluded in the last chapter. The significance of the problem and its proposed solution is explained according to the results found in chapter 5. There is also a suggestion for further work..

Chapter 2

Literature Review

2.1 Introduction

A brief discussion of the fundamentals of the image watermarking and segmentation is given in this chapter. Some basic techniques that are used for image watermarking and segmentation are also discussed in this chapter.

2.2 Image Segmentation

Image segmentation is referred to as the partitioning of an image into a group of semantically meaningful, uniform, and nonoverlapping segments with similar properties from the surrounds such as luminance, dimension, color, or structure. Segmenting images is a crucial first step in image analysis [5]. Brain tissues segmentation using MR scans is supposed to be extremely useful for diagnosing brain abnormalities, tracking diagnosis, and evaluating medication. Numerous automated or semi automatic approaches have been promoted as a way to reduce user intervention, however, their accuracy still seems to be lower than manual segmentation in the majority of situations [6]. Medical image processing, facial detection, pedestrians identification, and even more applications require image analysis techniques [7]. It's the process by which a computation turns an array of

adjacent pixels into parts containing consistent and homogenous properties from the original image analysis. Image segmentation has played and continues to play anoteworthy role in a variety of fields, from medicine to robotics.For example, segmentation followed by recognition or classification is compulsory for the automatic identification of malignant cells in digital mammograms [8]. Analyzing the image and retrieving information from this to execute tasks is a significant component of digital image technology, and the segmentation process is the preliminary stage. One of the hotspot areas of image processing and computer vision is image segmentation. To recognize an image segmentation of images is a precondition. It divides a test image across several related groups based on certain characteristics in terms of determining out what individuals are interested in.It also serves as a foundation for image evaluation, recognition, feature extraction[7].Large data volumes provide difficulties in medical image processing. As the volume of data expands, image processing and visualization methods must be improved. The development of scalable algorithms and advanced parallelization approaches has been enabled by the usage of graphics processing units [9]. Man-ual segmentation is effective in most circumstances but is susceptible to rater drift and bias, making it unfeasible for big datasets due to the repetitive and time-consuming nature of the process. Clinical applications provide better results with automatic segmentation methods if they have: Potential of segmenting as an expert,Exceptional results from a diverse variety of datasets, Processing speed that is realistic.Although expert segmentation cannot be considered 100 percent accurate in all circumstances,it can be viewed as a good starting point.Systematicperceptual faults are another potential, as are any kind of error induced by neglect that may emerge as a result of the tediousness of the segmentation operation [10].

2.3 Techniques of Segmentation

Over the last few decades, imaging has become a fundamental component of most applications in everyday life, necessitating the development of precise and reliable image segmentation techniques. Image segmentation is categorized into two types:

The term "local segmentation" refers to the process of dividing a particular re-gion or part of an image, Global segmentation, on the other hand, is focused on categorizing the entire image, that comprises many pixels. Segmentation methods can be classified into two categories centered on image properties: Discontinuity-based image segmentation (e.g., region segmentation) and similarity-based image segmentation (e.g., thresholding techniques, region growing techniques, and region splitting and merging fall into this category) [11]. This chapter will go over these segmentation approaches in detail.

2.3.1 Manual Segmentation Method

To perform manual-segmentation the radiologist has to use the multi-modality information provided by the magnetic resonance images, as well as structural and biological data acquired by training and practice. The technique requires the ra-diologist to observe many pieces of images, diagnosing the tumor, and precisely sketching the tumor states [12]. To extract the contour of the target structures. Typically, an experienced operator has gone through about eighty 512 * 512 images slice by slice. Manual segmentation allows users to completely use their medical knowledge, and if we trust the operator's proficiency, it is one of the most precise image segmentation algorithms.

As shown by numerous intra and inter-operator variability studies, Manual segmentation takes too long and is vulnerable to er-ror. Experts generated segmentation results sometimes measured as the ground truth. On the other side segmentation outcomes/results generated by experts are often difficult to regenerate, since even seasoned operators show considerable in-consistency in their previous mapping [5]. Based on similarity and discontinuity, image segmentation is categorized into two classes such as edge-based segmen-tation and region-based segmentation. Discontinuity-based approaches are edge or boundary-based, whereas those that rely on similarity are called region-based methods [13].

2.3.2 Edge Based Methods

Edge-based algorithms used rapid fluctuation in pixels intensities of an image because a single pixel intensity is insufficient for determining edge statistics [11]. Detecting the edges creates an edge image, which is then followed sequentially by edge pixels with adjacent neighbor connectivity and procured into a list to reflect an object boundary [14]. Edge detection algorithms locate edges at which intensity's first derivatives exceeds a particular level or the second derivative has no crossings. Edge-based segmentation algorithms identify the edges firstly, then determine whether or not to combine them to construct the boundary, which is then used to segment the appropriate regions [11]. The perimeter of the recognized boundaries needs to be about equal to that of the object in the input image for segmentation precision. This led to some other presumption: that every image's region of interest has a perimeter that may be recognized using gradient or second derivative methods [13]. Edge detection approaches include the Sobel operator, canny operator, Robert's operator, Laplacian operator, and others are used to detect edges [11].

2.4 Region Based Segmentation Methods

The region-based classification splits an image into segments that are identical or homogenous regions of associated pixels by implementing homogeneity requirements to all feasible groups of pixels. Some attributes, including colors, intensity,and structure, are shared by pixels in a region [13][15]. Most of the pixels inside the area of interest for the indexed segment, as well as the neighboring upper and lower sections subsequently transformed from the input data of composite spectral bands intensity values to an output vector[16].Region-based segmentation algorithms work iteratively by grouping pixels that are next to one other and have similar values together, and detaching groups of pixels that have different values. These strategies assume that the divisions produced are related to the objects or significant areas of image. Microscopy, computer -tomography (CT), Ultrasound,

magnetic resonance imaging (MRI), Positron Emission Tomography (PET), and mammography are among the images that cause challenges for segmentation approaches that use global information in an image [13]. Following methods are used to segment the image such as:

2.4.1 Seeded Region Growing

The most well-known approach for segmenting images is region growing,which is commonly used for medical image segmentation [17]. Region-growingis also termed as region integration or merging, this technique is utilized to extract aregion of interest of an image that is composed of collections of pixelsvoxels with similar intensity. Region-growing is also identified as region merger,which is atechnique for merging voxels with similar intensities.It starts with a seed point specified through an operator manually or by using an automatic seed finding tech-nique. Then, if the intensities are close enough, the region expanding or growing adds all pixel values to the increasing region (sustaining a predefined uniformity or homogeneity criterion).This process is repeated until the area can no longer accept any more pixels/voxels [18].Growing regions is an efficient strategy tosegment volumetric images that are a complete fabrication of massive interrelated homogeneous regions. As a result, in medical image processing, it can successfully segment various tissues,structures, and disorders from MR data.The growing re-gions may flow freely and overlap with non-interesting regions. if the origin pointthat is seed point and uniformity criteria aren't adequately defined. Furthermore, regiongrowing is susceptible to noise, and segmented areas may become detached or have holes in the presence of noise [19]. This technique has several advantages, including the ability to select several criteria concurrently and the capacity to produce excellent outcomes with less noise in the images. However, there are some drawbacks to this approach. For example, if the seeded area growing method is used, noise in the image may cause the seeds to be incorrectly positioned, and when the image is noisy or has strength differences, over-segmentation can occur [20].

2.4.2 Region Splitting and Merging Method

Image-Segmentation techniques such as regional split and recursively merge operations. Splitting is the practice of distributing an image into segments with relatively homogeneous properties, and merging is the process of combining adja-cent similar regions [11]. An image can be segmented by the users into a collection of random, disjointed regions and then combine or splitting the regions to satisfy the conditions of real image segmentation rather than selecting seed points [21]. At first, the variance of the entire image is computed. The image is divided into four quadrants if the variance exceeds the defined limit.Consequently, if any of these four quadrants' variance reaches the limit, it is subdivided into four more. This is repeated until the entire image is made up of a series of squares of different sizes, all with variances below the limit.

2.5 Thresholding Method

Segmentation of an image depends on thresholding seeks to split an image as input into the pixels with two or more values by analyzing the values of pixels to a specified threshold value T [13]. Throughout the images, the value of the threshold T will not change. Pixels with values less than T have been assigned to one category, while the rest were assigned to the other. On the original image, the boundaries between adjacent pixels in different categories have been superimposed in white. The output image X(y,z) can be derived from the original image P(y,z) using T as [11]:

$$X(y,z) = \begin{cases} 0, & P(y,z) < T \\ 1, & P(y,z) \geq T \end{cases} \tag{2.1}$$

Where P(y, z) denotes the pixel value at the specified point (y, z) [13]. Thresholding produces a binary image, with pixels labeled 1 corresponding to the object and pixels labeled 0 correspondings to the background.

2.6 Segmentation Based on Clustering Methods

Clustering is an unsupervised research method in which data items are divided into groups called clusters by remembering two characteristics: (1) high cohesionand (2) low coupling. According to the first property, data items belonging to one cluster must have a high degree of similarity. The second property specifies that data objects in one cluster should be distinct from those in other clusters [22]. The most widely used clustering techniques appear to be K-means clustering, FCM clustering, and the expectation-maximization method [23]

2.7 ANN Based Image Segmentation Techniques

An Artificial Neural Network is a biologically inspired computational model which is composed of functions and neurons. The model requires training before it could solve a problem. The ANN model can be trained to produce output that is analogous to what is predicted [24]. It's more difficult to say which training method has been the most effective or precise for a given situation. Since multilayer learning machines have been known for a long time, however, their efficient im-plementation for practical tasks has been hindered by the lack of suitable training algorithms [25]. Following are the factor that influences the training of network including the problem's complexity, the quantity of datasets in the training phase, the network's connection weights and bias values, the error goal, or even though the network is deployed for object recognition or prediction of function [25]. ANN has investigated several training algorithms, including the Powell-Beale-Conjugate Algorithm,Polak-Ribiere-Conjugate-Gradient Algorithm, Levenberg-Marquardt, Scaled-Conjugate-Gradient Back Propagation, Resilient Back Propagation,One-Step-Secant Back Propagation,Fletcher,ReevesConjugate-Gradient Algorithm, and Quasi-Newton Algorithm with (BFGS). To find the best training algorithm, the identical structural parameter setup is used to train each neural network ar-chitecture [26].

2.8 Related Work for Image Segmentation

The volume of MRI data sets is growing exponentially from day to day. As a result, it is essential to accelerate medical image processing and disease diagnosis technologies while sustaining a higher degree of accuracy.In this context, the researcher has proposed various segmentation techniques with widely differing degrees of accuracy and complexity in the literature discussed below.The author of the study [27], provided a review regarding the most often used segmentation and classification approaches for brain MR scans from the year 2014 to 2019.In addition, the author presented a hybrid strategy for Medical image processing.The authors used a feed-back pulse-coupled neural network as a frontend processor to segment images and discover ROI, then used the DWT toretrieve features from the MRI dataset. After that, the wavelet coefficients'dimensionality is reduced using PCA, leading to a further precise and effective classifier.

The condensed attributes are directed to a back-propagation neural network, which uses feature selection parameters to identify inputs as normal orabnormal. The author of the study [27] performed experiments on Axial, T2weighted, 256–256 pixel MR brain images. The dataset was obtained from the Harvard Medical School website. The model achieves a classification accuracy of 99 %, with a sensitivity rate of 100%and a specificity rate of 92%. The study concludes that the suggested classifica-tion approach will effectively discriminate among balanced as well as pathological cases, improving the accuracy of human brain disease diagnosis. The author of the study [28], proposed a system by using FCM for segmentation and classification of a brain tumor as benign (notspreadable) or malignant (spreadable and contains cancerous cells). FCM is a soft clustering technique based on fuzzy set theory. Each pixel in a image canbe classified into multiple groups. pixels are consigned toward a class according to a definite association value. The algorithm's execu-tion time(s),MSE, PSNR,and segmented area (pixels) are all found as evaluation parameters. The mean square error is the collective square error concerning the compressed and original image, while the peak signal to noise ratio indicates the amount of the peak error.

The excellence of the compressed or reconstructed image will be better if the value of PSNR is higher. Wavelet coefficients in an MR image are extracted using a DWT. It is a type of linear transformation that is used to convert an input data vector into another vector. It splits the data into various frequency components such as HH, HL, LL, and LH. In the study [28], it is utilized to extract image features. because its multi-resolution diagnostic property helps it to analyze an image at various resolutions. Then the PCA is used to reduce dimensionality. It's used to reduce the dimensions of data by selecting the most appropriate from a wide pool. As a consequence, a new function matrix with reduced dimensionality is retrieved.

The dataset is then translated to GLCM and arithmetical features in-cluding mean, standard deviation, entropy, variance, and so on are extracted. For the SVM training process, the extracted feature database is used. The authors of the study used a private dataset of brain MRI and found that the proposed automated method had 98.82% accuracy, 100% sensitivity, 97.83% precision, and a 1.17% error rate [28]. In another study Song et al [29] , presented a modified scheme of FCM that is MRFCM. This technique incorporates the spatial infor-mation of neighborhood pixels and has strong anti-noise capability. The author of the study [29] applied the MRFCM algorithm on three types of data set such as synthetic-images, simulated brain MRI images, and real brain images, and af-ter that, the results have been associated with typical FCM results.The author of the study [30] proposed a framework for fully automated segmentation of MR brain images.

A three-step segmentation approach is used in the framework. First, non-brain structures are removed which is also known as skull stripping by using the level set method. After that, the non-uniformity rectification method then uses approximations of tissue strength discrepancy to recompense for non-uniformity. Finally, it employs a statistical model relying on Markov random fields (MRF) for MRI brain image segmentation, also known as brain tissue classification. The brain tissues are categorized into the cerebro-spinal fluid, white-matter, and gray-matter..The author of the study [30] experienced the anticipated framework both on simulated and real MR images.Kong et al. [31] established a technique for segmenting the skull.

The authors used pre-processing techniques such as wavelet denoising to obtain the precise features of the skull and various tissues such as WM, GM, and CSF. CNN is executed for the automatic segmentation of images. The authors of the study [32] also used parallel computation to accelerate the entire process. The author of the study [32] measured the percentage of each brain tissue, which can be used to diagnose various disorders (e.g., cerebral atrophy), which is mostly caused by a decrease in GM or WM brain tissue. Experiments in the study [32] were carried out on a private dataset, and the findings were compared to the VCH model, yielding an accuracy of over 90%.Khorram et al. [33] implemented the segmentation of gray matter (GM), white matter (WM), cerebrospinal fluid (CSF), and thalamus (large mass of GM) from an MR brain image. The author proposed an enhanced thresholding technique for segmenting MR brain images using the ACO technique. The researchers proposed the scheme in [34], which used textural features for heuristic details, as well as post-processing image enrichment to accomplish improved output based on homo-geneity. The authors of the study [33] experimented with the BRATS-2012 dataset and achieved accuracy up to 97%. The authors compared the accuracy of work with PSO, K-means, and EM approaches using 20 MR scans.

2.9 Related Work for ANN Training Algorithms

To train ANN, an effective training algorithm must be predicted. Prediction of training algorithms to train ANN has been a major topic in research. Many at-tempts have been made to produce a realistic algorithm capable of accurately predicting with a high degree of accuracy. The ANN employs a variety of training functions. An optimum training function must be used in the ANN to predict the least amount of error.

The literature listed below contains the work of many schol-ars who compared training algorithms and recommended the best one based on their findings.The author of the study [35] proposed a model for forecasting the categorization of soil types, and the optimum neural network training algorithm was found.A repository of the 120 soil prototypes was employed in the study. To train the neural networks

batch-gradient-descent training, batch-gradient-descent training with-momentum, variable learning speed Scaled-conjugated gradient, Fletcher-Reeves conjugated gradient, Pollack-Ribier-conjugated-gradient, Paul-Bill-conjugate-gradient, quasi-Newton (BFGS), quasi-Newton, one-step-secant, and Levenberg-Marquardt conjugate gradient. The RMSE, CRM, and COD were used to assess the efficiency of the proposed model. By comparing actual and predicted values, the Levenberg-Marquardt algorithm with COD = 99.88% and RMSE = 0.0521 is the best training method for predicting soil type classification. Then the back-propagation method and quasi-Newton BFGS can accurately train the network. It's worth noting that the data used in this study was limited. When the quantity of data points in a neural network is increased, the accuracy of the training can greatly improve. The author of the study [36] looked at how artificial neural network (ANN) modeling techniques could be used to predict the properties of waste tire steel fiber reinforced concrete (SFRC). For training, five ANN algorithms were investigated, namely incremental-backpropagation (IBP), batch-backpropagation (BBP), quick-propagation (QP), Levenberg-Marquardt-backpropagation (LM), and genetic algorithms (GA). In descending order, the ANN training algorithms' predicting ability performance was GA , IBP ,LM ,BBP and QP. Constructed on statistical metrics of performance such as Root Mean (R), Root Mean Square (R2), and AFV, for analysis and forecasting the strength of concrete fiber reinforced derived out of used tires, the Genetic-Algorithm (GA) was considered as the optimum approach. According to the findings, backpropagation is not as effective as the genetic algorithm (GA) iterative method. As a result, this study finds that choosing the correct learning algorithm is crucial to simulate inputs using ANNs effectively and that using a Genetic-Algorithm to achieve high prediction efficiency is extremely suggested in ANN modeling [36]. Author of the study [26] The study's authors developed an artificial neural network model to approximation the compressive power of concrete using an optimal dataset of representative concrete mix proportions. Based on the eight distinct training techniques, eight separate neural network models are constructed; each artificial neural classifier is trained with the very same structural configurations. LM is the most feasible possible training method, with R (correlation) equal to or better than 95%, after LM, BFG seems

to be another credible training function with the same architecture and design parameters on average, considerably better than 93% on average. The ANN models are repeated with other activation functions realistic to the hidden layer neurons, such as tangent-sigmoid and log-sigmoid functions. One of the best available tools for predicting concrete compressive strength is an ANN model using the learning function Levenberg–Marquardt (LM).The author of the study [37] conducted research in which they optimized an ANN model for predicting Polymeric Inclusion Membranes (PIMs) Cr(VI) removal ef-fectiveness by using the right training algorithm. The outputs from the created models and dataset acquired from laboratory experiments forecasting of PIMs Cr(VI) removal efficiency are assessed, compared to discover the optimal train-ing algorithm. The predictive ability of ANN models constructed and trained using three different methods comprising Levenberg-Marquardt (LM), Bayesian-Regularization (BR), and Scaled-Conjugate-Gradient (SCG), was evaluated [37]. Based on this computation, LM was discovered to be the superlative learning algo-rithm for PIMs Cr (VI) removal efficiency estimates. The LM training algorithm outperformed the BR and SCG in predicting PIMs Cr (VI) removal effectiveness is calculated using six inputs: time, extraction type, extraction quantity, density, polyester type, and polyester amount, as demonstrated by R2 values of 0.97, 0.95, and 0.72 in test dataset for LM, BR, and SCG, accordingly. Lastly, each training method's precision of prediction ability was investigated, yielding the following results: For train, validate, and test data sets, LM ,BR and SCG is the preferred method [37].Jaiswal et al. [38] studied the impact of several training strategies for ANN on the feedforward backpropagation architecture. For analysis, MATLAB R2017a is used to design and run the training algorithms. Several training algorithms are used to achieve the greatest level of accuracy between expected and definite results. The study is based on the Kaggle dataset for housing price prediction.

This study concluded that if network training must be finished quickly, the Scaled Conjugate Gradient technique should be employed; but, if a small error cannot be tolerated, the Levenberg-Marquardat approach should be utilized at the cost of additional time and processing power.

To separate the targeted images from the background, Wencang Zhao [39] sug-gested approach for the segmentation of images that is truly based on textual features[40] and [41]. The images from a micro-CT dataset are used.As a pre-processing phase, a de-noising filter is used to eliminate noise from the image. Next, feature extraction is conducted, followed by the creation of a BPNN, and finally, weight number of network is modified, and the result is saved. Threshold-ing and Region Growing methods are compared to the proposed technique. The results reveal that the suggested strategy surpasses previous methods in terms of segmentation speed and accuracy.

Lijun Zhang [42] proposed a new colour image segmentation algorithm based onneural networks. They proposed SOMNN, a new approach that combines Wavelet Decomposition with Self-Organizing Map (SOM). The parent pixel was chosen by a vote among the child pixels. Following initialization, the ANN discovered a segmentation result that satisfied all levels. To eliminate noise, wavelet decomposi-tion is used. As a result, wavelet decomposition and SOMNN are used to segment data. The approach reduced noise and produced accurate segmentation, accord-ing to the results. Image Texture Classification using Artificial Neural Networks was proposed by Shohel Ali Ahmed [43]. At first image is collected and prepro-cessed, after that, feature extraction [44] is conducted, and texture classification is performed using an ANN classifier [45].Clustering is used to distinguish the backdrop from the sub-images. The input pixels are combined into two clusters using a trained ANN, which produces results. It creates texture categorization and image segmentation.Image segmentation approaches were defined by Pal and Pal [46] as:thresholding for grey levels, Pixel categorization that is iterative, segmentation of the surface, segmentation of colour images; as well as identification of edges.Author in [46] described iterative pixel classification techniques that is based on neural nets. Only FFNN-based approaches for MRI segmentation were reviewed in [47]. The supervised and unsupervised NN-based image segmentation approaches reported in the literature can be split into two types. For segmenta-tion, supervised approaches necessitate the use of a human expert. Algorithms

that are Unsupervised or clustering procedures that either semi automated or completely automated. To increase the effectiveness user participation may be required at some point during the process, but the outcomes should be more or less human independent.Without the need for manual involvement,an unsupervised segmentation approach splits the images.However, application-specific a priori knowledge, such as anatomical, physical,orbiological understanding, may be used to create these systems at design time. Multi-layer perceptrons are the most basic NN architecture for image segmentation (MLP). Blanz and Gish [48] succeeded in segmenting grey-level images using a three-layered perceptron. The image segmentation challenge was reduced to a pixel classification problem using their BPNN technique.The vector of characteristics retrieved from each pixel served as the input vector for the ANN, while the output vector was the vector of classes for segmentation.The network was trained using a traditional back-propagation (BP) learning algorithm. Author in [49] employed a supervised tech-nique based on BPNN to segment GM,WM and CSF magnetic resonance images derived from spinecho. The image's histogram was utilised to train a BPNN. The percentage of grey or white matter in the image was the architecture's output. Hopfield presented HNN as a solution to optimisation difficulties in 1985. Each neuron in an HNN is connected to the next., also the weights are balanced. The optimization network relaxes into stable states that minimise an energy function of the form [50][51] [52].

$$E = \sum_{i=1}^{N} \sum_{j=1}^{N} w_{ij} v_i v_j - \sum_{i=1}^{N} I_i v_i \mid \tag{2.2}$$

In which N is the number of neurons, vi denotes the neuron's output that is onI th, and Ii denotes the I th neuron's external input. Hopfield established that HNN relax into a stable state with the goal of minimising the energy function that corresponds to it. In [53] The neural network of a fractional order Hopfield type exponential stability also investigated.The equilibrium point's exestence and uniquness are demonstrated first. Then, the use of the Lyapunov function,a requirement for the the stability of equilibrium exponential is also found.

Various values, the validity of their criterion is supported by numerical examples . For MRI segmentation, Author in [54] used an HNN with winner-take-all (WTA) neurons. The image was divided into Nxk neurons, with N denoting the total number of pixels in an image and k denoting the amount of classes available or regions. Network can minimise an energy function of shape by using T2-weighted and density-weighted MR images of the skull.

$$E = 1/2 \sum_{k=1}^{N} \sum_{l=1}^{N} R_{kl} V_{kl}^2 \tag{2.3}$$

Rkl denotes the gap between the kth pixel, the class l barycenter, and kth neuron in class l produces Vkl as its output.Author in [55] suggested a system based on anatomical or biological information as well as images production physics.The input image is changed using image generation physics, which improves the image's signal-to-noise ratio by enhancing information linked to signal decay.Anatomi-cal knowledge is also employed to create an initial segmentation of the original images.The segmentation is then performed using the images generated by the neural classifier.Constraint Satisfaction Neural Networks are a novel type of neu-ral network proposed by Author [56] for images segmentation (CSNN).The idea behind this method is that an image segmentation problem may be characterised as a Constrained Satisfaction Problem (CSP).The process of providing a label to each pixel based on particular spatial limitations is known as the segmentation issue.A CSNN is made up of n.n.m neuron s, In which n.n represents the images dimension and the m shows how many classes there are.(or labels) into which the objects must be split. Each neuron is linked to every other neuron in its vicinity (8 connections).The spatial limitations on each pixel's segment label are represented by these connections.A CSNN is made up of a collection of items, a collection of labels (classes), and restrictions on space that describe the connection between items based on neighbour relations.They are updated such that a neuron will activate neurons in the same class while inhibiting neurons in other classes.To deal with the crossover between segments, a winner-take-all system is selected.There are two steps in this method, much like in normal learning algorithms:learn-ing and categorization. Each of the seventeen neurons in the network receives the feedback

from its own output as well as excitatory/inhibitory signals from its neighbours. This method necessitates knowing the number of classes (labels) ahead of time. The proposed method also necessitates the assignment of label probabilities to each pixel at the outset, utilising algorithms like Kohonen's self-organizing map, K-means, ISODATA,fuzzy c-means (SOM).

Terman and Wang [57] proposed a globally inhibitory oscillator network that was locally excitatory (LEGION) as an image analysis and segmentation computational technique.The principle of temporal correlation underpins LEGION's concept and originates in the biological world.The neurons of the visual cortex respond only to stimuli that originate in a specific area of the visual scene.

Furthermore, synchronised behaviour across geographically dispersed neurons has been seen, with cortical neurons correspond-ing to a specific homogeneous area oscillating in phase while neurons referring to different areas 18 oscillating out of phase. By attaining quick synchrony with local excitation, LEGION is able to group comparable features in an image. Further-more, desynchrony with global excitation/inhibition separates distinct features. Chakravarthy et al. [58] developed an ANN of complex-valued neurons that ex-hibit stimulusspecific oscillations for images segmentation. The synchronisation of brain oscillations, according to their hypothesis, is achieved by both neuronal cooperation via excitatory/inhibitory couplings and hebbian-like synaptic modu-lation. As a result of the input images, the networks exhibit coherent oscillations, with segmentation happening due to local uniformities in image intensities.

They propose that unique local characteristics such as texture and orientation For med-ical image segmentation, author in [59] employed a single layer LEGION-based neural network.The image pixels and neurons are linked in a one-to-one rela-tionship. Pixels with comparable properties will cause their respective neurons to exhibit oscillatory behaviour, and their phases will function in synchrony, thanks to the dynamics of the LEGION design. On CT scans, rather than MR images, their adaptive strategy for grouping comparable characteristics (intensity contrast of pixels), has proven to operate better. Classic segmentation techniques, such as statistical methods, global thresholding, active contours-snakes, and so on, were 10 times faster. This design can be made more flexible by adding a second layer

to handle the results of the first layer, resulting in better segmentation results.To segment range images, author in [60] presented an architecture that included LEGION and PCNN. Each neuron in their ANN has excitatory lateral connec-tions to its neighbours as well as a global inhibitor link. A feature vector with depth, surface normal, mean, and Gaussian curvatures is associated with each neuron. There is no need to know how many regions/segments there are in ad-vance.

The performance of various ANN training algorithms in the architecture with feedforward backpropagation is investigated in this [61] paper.For the analy-sis, MATLAB R2017a is used to design and run the training algorithms. Different algorithms for training LM algorithm, Gradient Descent algorithm ,Scaled Conjugate Gradient algorithm ,One Step Secant Backpropagation algorithm ,Bayesian Regularization algorithm and Broyden-Fletcher-Goldfarb-Shannon algorithm are examined to determine the degree of accuracy between the desired and actual outcomes.

The research is based on a Kaggle dataset for housing price prediction. It was determined that if network training must be finished in a short amount of time, the Scaled Conjugate Gradient algorithm should be employed; however, if a little amount of error cannot be tolerated, the Levenberg-Marquardat technique should be utilised at the cost of additional time and processing power. In [61]five genetic algorithm have been tested. Each training algorithm's degree of generalisation or precision of predictive capacity was assessed,and their ability was graded in the following order: IBP, BBP ,LM ,QP,GA.this paper concluded that increment and batch backpropagation (IBP, BBP) methods of gradient de-scent backpropagation can be used as the best training algorithms for modelling and forecast of in vitro drug release patterns.

For multi-scale image segmentation based on pixel classification, author in [62] developed a Kohonen neural network . Different geometrical invariants features were assigned to each pixel. The features vector was fed into a Kohonen neural network.The architecture was practised using a training image. Any image that looks similar to the training image can be segmented by comparing the feature pattern representation of each pixel. As a result, supervised labelling was used to categorise pixels into classes.

Author in [24] investigate the possi-bilities for employing artificial neural networking as a machine learning technique to estimate flood predictions by obtaining data from multiple sources. Flood fore-casting models were constructed using five modern NN computational approaches and 5 different trainingalgorithms:Bayesian-Regularisation algorithm (NNbr), Levenberg Marquardtalgorithm (NNlm), Conjugate-Gradient algorithm (NNcg), Resilient-Backpropagation algorithm (NNrbp), and Scaled-Conjugate Gradient al-gorithm (NNscg).

All of the models were evaluated using statistical measures such as MSE, root means square error (RMSE), coefficient of correlation (R2), and abso-lute average deviation (AAD). The following is the sequence in which the models' MSE values increased: NNlm , NNscg , MLR , NNcg ,NNrbp and NNbr.

The best model for predicting floods was the NNlm model. The Levenberg–Marquardt model was found to be more predictive and trustworthy. When the NN findings are compared to the MLR results, it is evident that the NN has a significantly higher predictive capability [63].Another study conducted in [25] found that the precision of MLP, that employed in several neural applications, is completely dependent on the learning algorithms used.

Even though multi-layer perceptron is not frequently utilized for image organization, the results reveal that some MLP training algorithms are just as good as other network topologies in terms of providing a solution. The outcomes demonstrate that the 'trainlm' method outperforms MLP on feature extraction data from the vision group. The 'trainbr' algorithm is effective, nevertheless as good as the 'trainlm' approach.

2.10 General Watermarking Approaches

For the transmission of a message in a secured environment, the process begins with a candidate image .The candidate picture might be treated as pure noise, noise with additional information, or a multimedia message. The watarmarked data travels across a communication route that is potentially lossy, noisy, or un-reliable. As a result, the watermarked data may be subjected to attacks such as lossy compression, geometric distortion, signal processing operations, and signal

conversion, among others; that is, a discrepancy between the original watermarked data and the received data may exist. Image with watermark travels over a noisy route of communication. The average information included in an image has more uncertainty or ambiguity because to noise by maximising the information entropy. As a result, Techniques for watermarking are limited to on images with high resolution and intricate patterns with a greater information entropy. As a result, in order to boost safety, the images that has been encoded should treated in a way that rebuilding an image is stable. In the input as well as the Fourier planes, a novel approach for encoding visual images acquires the images that has been encoded using a irregular encoding methodology, Two deformable mirrors replace the two randam phase-plates at the input and fourier-planes, respectively. As a result, the machine can shape the image's amplitude and phase data in whatever way it wants. Digital images, watarmark embedding and a watermark extraction component make up a watermarking technology in order to create a secure communication paradigm.

The cover images is first pre-processed in the watermark embedding section, the image's integrating ability information is obtained by cal-culating its sensitivity. Using an optical image encoding method and a secret key, the coder then integrates a watermark images into the high density value of the in-put images. The system then generates the watermarked image after obtaining the details on an infrared-light's magnitude and phase adjustment.Figure below il-lustrates watermark embedding process. Watermarked image finally pre-processed during the watermark extraction step. The system then extracts the laser beam patterns' amplitude and phase shaping data. Following that, these light patterns ' complexity is assessed. In order to achieve improved robustness and impercep-tibility, The watermark is extracted using a high entropy value.. The watermark image is recognised as an output from the watermarked image by a decoder that uses the same key as the watermarked image. The method demonstrates that reconstructing a watermarked image from a watermarked image is simple, reli-able, undetectabl.Figure 2.1 and 2.2 shows embedding and extraction process of watermarking.

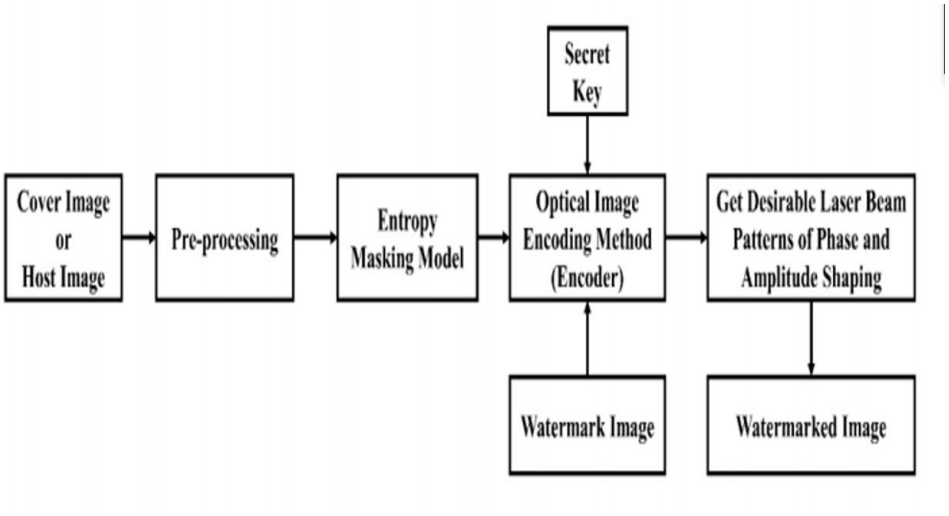

FIGURE 2.1: watermark embedding [64]

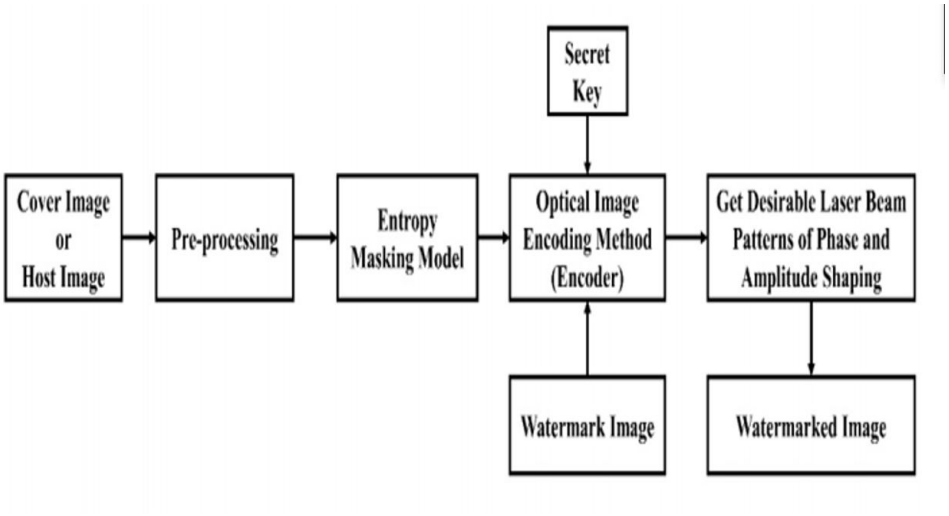

FIGURE 2.2: watermark extraction[64]

Discrete Fourier Transform , DCT and DWT are the most common frequency domain approaches (Discrete Wavelet Transform). DCT algorithms have low arith-metic complexity and are more resistant to JPEG compression attacks.With regard to DCT-based watermarking methods, two important issues should always be considered: the first is determining DCT coefficients the image watermark is perceptually undetectable when high-frequency coefficients are used., A filtering procedure on the image, on the other hand, removes the watermark. Second diffi-culty is quantity of DCT coefficient values changed to add the watermark into the image.

The watermark invisibility will be affected by the DCT coefficient values modified, and the image may be ruined to a large amount.

2.11 Existing Techniques of Digital Image Watermarking

Digital watermarking consists of several different techniques for protection of digi-tal content [4]. The digital image watermarking falls in two main broad categories:

1 Spatial domain techniques

2 Frequency domain techniques

Techniques of watermarking are shown below in figure 2.3.

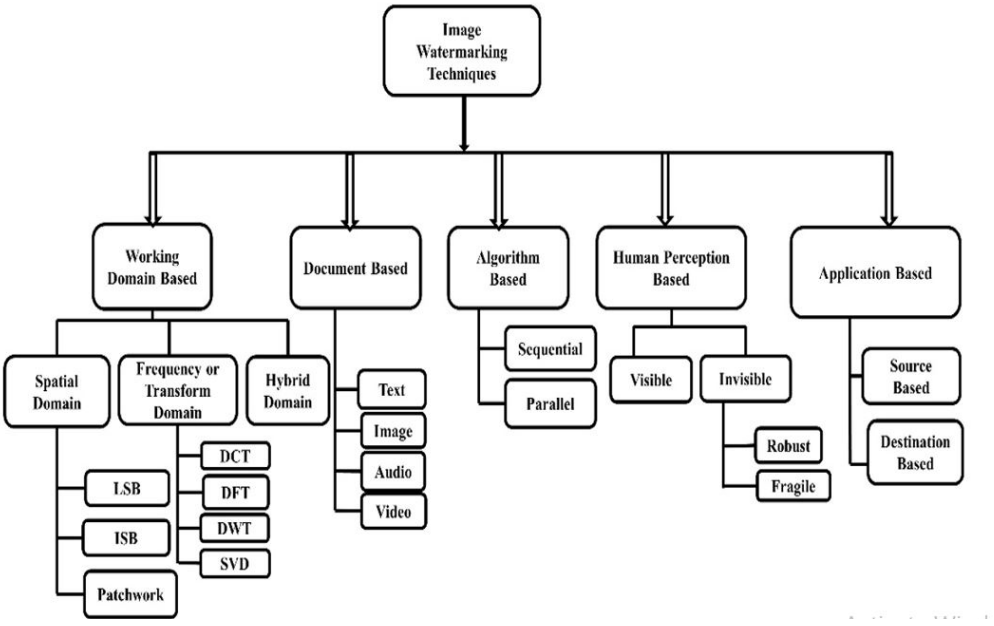

FIGURE 2.3: Techniques of watermarking [65]

2.11.1 Spatial Domain Watermarking

Spatial domain techniques works on pixels and pixel value are modified for embedding the watermark. The commonly used spatial domain technique is LSB.Whereas

frequency domain coefficient are modified by Frequency domain techniques for embedding watermark. DCT, DWT and DFT are commonly used frequency domain technique. In case of robustness and imperceptibility, frequency domain techniques are more reliable than spatial domain technique. Based on the pixel intensity the resulting watermark could be visible / invisible. We look at a number of spatial domain techniques that have sparked the interest among researchers because of their optimal mix of imperceptibility , resilience, and capacity, which are the three most important requirements for every watermarking methodology. Strategies are simple to use, efficient, and quick to execute. Furthermore, the image The watermarked image's property could altered. These techniques, however, only work successfully if the images been manipulated by humans or hasn't been subjected to any noise. Trimming the image removes the water-mark, which is a major weakness in spatial domain watermarking. These tactics embed a substantial quantity of data in terms of capacity yet the inserted data may be easily spotted by many assaults.A little piece can be inserted multiple times as well. As a result, even though the rest of the image has been destroyed due to numerous attacks, a single remaining water-mark will be considered a success. Different watermarking techniques are discussed in [64]

2.11.2 Least Significant Bit

The most used spatial domain watermarking mechanism is the LSB. The LSB of some pixels can be altered to conceal the MSB) of some other. Using a certain key, it generates a random signal. The watermark is injected in the LSB and can be removed in the same way. The host image can be processed using a number o different methods. This is a simple and easy to implement algorithm. Because the least significant bits contain less meaningful data, the The quality of the cover host is unchanged. It does have a good level of perceptual clarity. while having little effect on the host image. However, unwanted noise, cropping, lossy compression, and other factors can affect this algorithm, and a hacker can easily modify the

embedded watermark by setting all of the LSB bits , figure2.4 depicts an example of LSB.

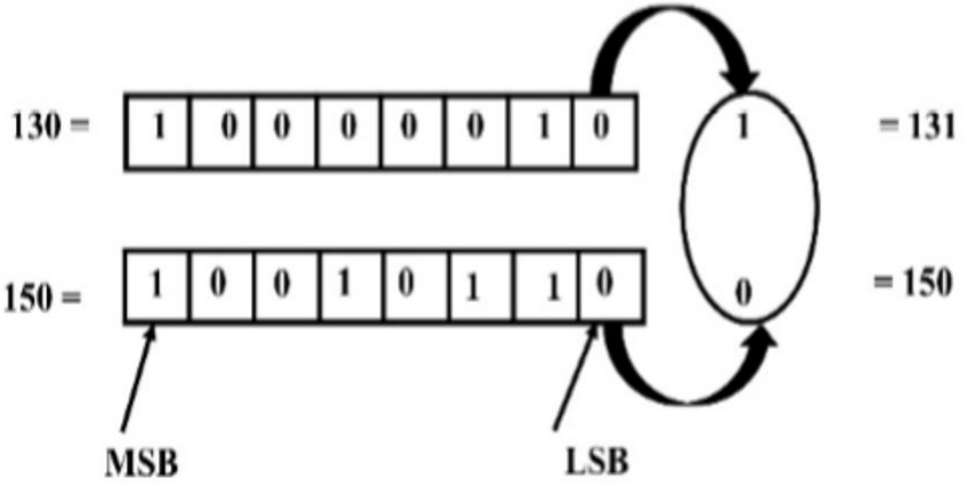

FIGURE 2.4: Least significant bit[66]

Several studies have looked on LSB modifications that are frequently associated with the spatial domain. On the basis of a bit-plane of digital discrete signals, LSB techniques have been created (e.g., audio or images). A signal is represented by a bit plane, which is a group of bits in each binary integer that all have the same bit location. One bit-plane is used by the bulk of embedding strategies. Others are using three or even four bit-planes for embedding with appropriate images quality, however this strategy only functions on the least significant bit-planes .The 4 least significant bits can be replaced with the selected bit of the concealed images by simply using an OR operation in a specific method [66]. This methodology turns the host images to a binary bit stream, then sets the embedded bit to zero and shifts the hidden image 4 bits to the right. The OR procedure is then applied to these two images to create a composite image.

2.11.3 Intermediate Significant Bit

Although a LSB approaches are most common and straightforward modern watermarking approaches in the spatial domain, attacks resistance is not assured. As a result, different approaches, to improve the watermarking service's resilience

and quality, approaches such as intermediary significant digit (ISB) methods havealready been developed ISB approaches based on various algorithms have been developed in several studies. Each of these methods uses ISB instead of the standard LSB method, determining the optimal pixel value here between range centre and edge.The watermark cover image is protected from the numerous variety of attacks, and changes to the watermarked image are kept to a minimum with this method [65]. Another study [67] looked at the double intermediary signifi-cant bit (DISB) approach, that entails embedding 2 bits within each pixel of the input images and updating the initial pixel with the remaining 06 bits. If the actual and inserted images differ, the watermark image can be picked by choosing the value of each pixel that is nearest to the source.When compared to LSB approaches, the suggested model yields a image with a higher resolution and a watermark. As a result, the DISB approach ensures strong attack resistance while also improving image quality. Resiliency and quality are the two foremost critical aspects of any watermarking system, which may be assessed using fair normalised cross-correlation (NCC) values. In the spatial domain, ISB approaches have been employed for image watermarking. This approach substitutes original image pixels with watermark pixels by keeping the watermark pixels next to a full or empty portion in the actual images pixels. The original-images file pixel is added outside any of the range's edges after the watermark pixel value is validated against each bit-range, plane's, and bit-range's. In grayscale images, there are 08 bit planes: the first retains the MSB, the eighth holds the LSB is used, and the leftover bit planes are used as ISB. Figure 2.5 represents intermediate significant bits .

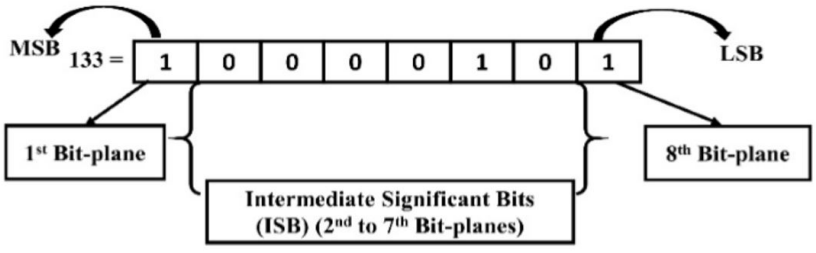

FIGURE 2.5: Intermediate significant bit [67]

2.11.4 Patchwork

Patchwork is a pseudorandom statistical procedure which embeds itself invisibly into an original image by using repeated pattern encoding using a Gaussi and is tri-butio The first-patch's image data is dimmed, whereas the second patch's image data is darker.Non-geometric images alterations are more resistant to patch-work approaches, and the process is independent of the original image's content [68].In this situation, Before decoding, the code can be destroyed due to scale, trans-lation, or rotation , and additional affine coding, feature recognition, or both can improve the robutness.Although patchwork is impervious to cropping, it loses precision as a result. The original image is the pseudo-random bit stream. The pair is encoded with a bit of information, with d deno-ting the difference between the two pixels, the encoding is 0 for d 0 and the pixels are swapped f or d 0 The next pair can be advanced if d is equal to zero/ greater than a predefined threshold [69].

As a result, the brightness might be raised in one spot while being diminished in another.This method works well with vast swaths of texture is random, but not with text im-ages.Section of the image with a random texture pattern is duplicated to another a texture-matching portion of the image Each textural area is recovered using auto-correlation. [70]. publication, based on additive and multiplicative patchworks, a general patchwork approach was suggested [71].This method embeds and detects the watermark using statistical data.This approach employs the location-shift and scale-shift schemes to detect watermark data.Their proposed approach has been demonstrated to be resistant tocompression attacks.

However, the patchwork method's robustness against multiple attacks is very great;only a limited quantity of data may be hidden [72]. The watermark can be inserted in an image using redundant pattern encoding, and it canbe removed by a private key related to the decoding process.

2.12 Frequency or Transform Domain Watermarking

Watermarking approaches for the spatial domain are too sensitive, as they can be exploited with ease . In comparison to frequency-domain algorithms, these strategies are substantially less resistant to many forms of attacks. These flaws have prompted researchers to investigate transformdomain watermarking approaches, which, rather than hiding data in time, effectively hides data in the transform space of a signal. In order to represent a images in the frequency domain, this approach translates it using a pre-defined transform.The water-mark is then embedded by altering the wavelet transform values of the actual images with numerous transforms, including the Discrete Cosine Trans-formDCT, Discrete Fourier Transform DFT, Discrete Wavelet Transform DWT, Singular Value DecompositionSVD, Hadamard, CAT, FFT, PHT, and Fresnel transform, among several others .Finally, it uses an inverse transformation to ex-tract the water-mark with the help of a valid key. The above technique is depicted below Phase shift information should be added to every sinusoid of the images in order to recover the input signals in frequency domain [73].Figure 2.6 frequency or transform domain watermarking.

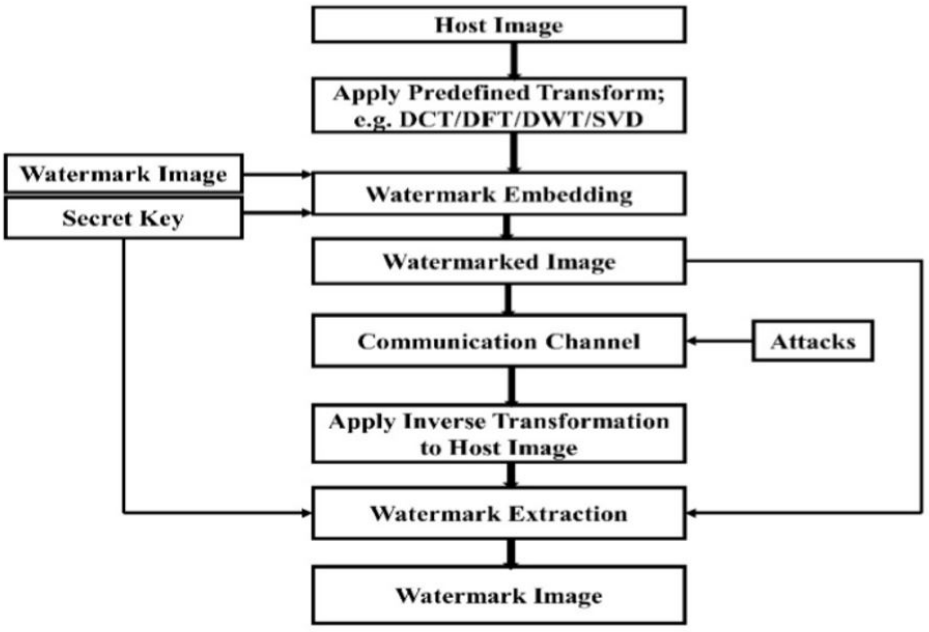

FIGURE 2.6: Frequency domain watermarking [73]

Many studies on transform domain images watermarking have been conducted, demonstrating its better robustness, security, and imperce-ptibility against a vari-ety of attacks including compression, noise, filtering, chopping, and rotation. This part examines research that employed frequency domain transfer techniques such approaches.

2.12.1 Discrete Cosine Transform

The discrete cosine transform divides a images into identical frequency coefficients by changing frequency components, which can be expressed as a sum of cosine functions. A DCT is a Fourier transform using a limited number of data points. Only actual numbers are permi-tted to be used here.The usefulness of the DCT coefficient is determined by its variance. For example, with the JPEG image format, DCT is crucial for image reduction.

In the DCT domain, many studies on digital images watermarking technologies have previously been conducted. Block-based DCT image watermarking is one of them. It works by splitting the cover image into numerous image pieces and applying the DCT transform to each of them individually.

The watermark is then injected into the block and DCT based cover image using an approach.The water-marked image is then created using the inverse discrete cosine transform (IDCT). Figure best describes the above-mentioned DCT approaches for watermark em-bedding.

It's worth noting that watermark extraction can also be done the other way around. Figure best describes the above-mentioned DCT approaches for watermark embedding. It's worth noting that watermark extraction can also be done the other way around.Figure 2.7 represent discrete cosine transform

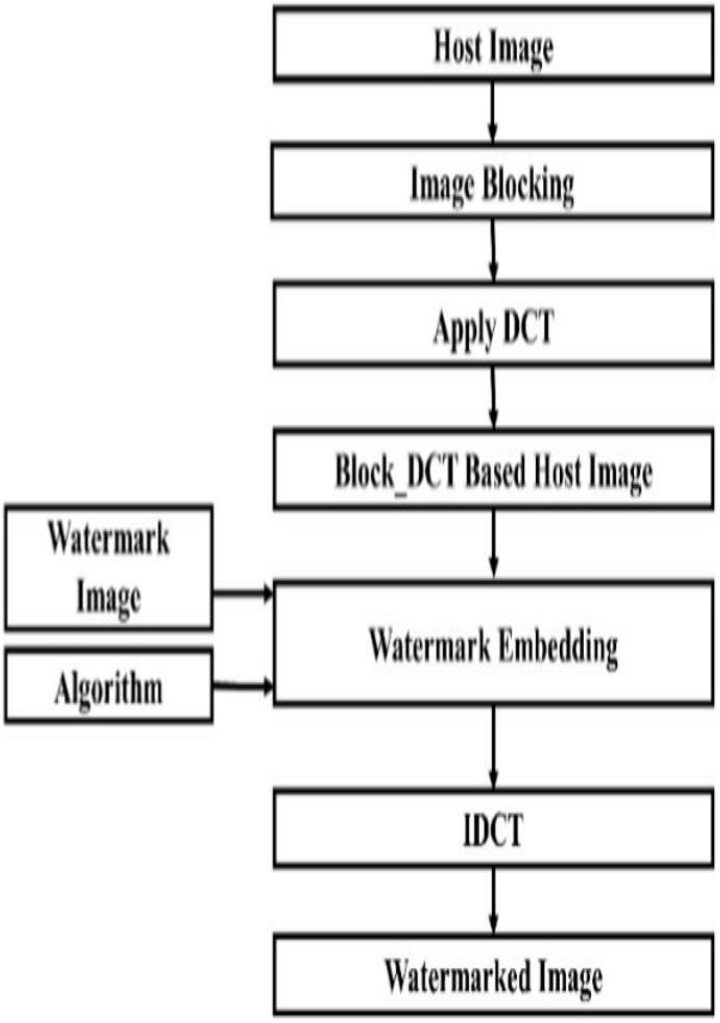

FIGURE 2.7: Discrete cosine transform [74]

Roy, Pal, and colleagues [74] developed a DCT-based colour watermarking method for embedding numerous copyright ownership and validity watermarks.. By addressing fundamental shortcoming of block based DCT approaches, namely blocking artefacts, the system displayed superior robusness and imperceptebility were improved, and the PSNR value was increased.Using an error-correcting code, one

watermark bit was saved (ECC). The system, on the other hand, had a high computational complexity.

2.12.2 Discrete Fourier Transform

The discrete Fourier transform DFT employs samples that are evenly spaced.In this scenario, the discrete-time Fourier transform converts a series of fixed length numbers of spaced evenly samples of a function together into series of equally spaced samples of the same length (DTFT). The DTFT makes use of a set of com-plex (magnitude and phase) exponential functions which are coupled harmonecally.

The DFT produces a discrete and periodic signal by representing the source frequency domain input series. Signal processing, image processing, filters, convolu-tion operations, sinusoidal spectrum analysis, and Fourier analysis are just a few of the uses for DFT. Many studies on the DFT for images watermarking have been conducted [75] developed two multidimensional Fourier transform-based colour image water-marking techniques. A colour water-mark was embedded using the spatial-chromatic discrete Fourier transform (yellow and blue).

In this method, chromatic information in a colour image is transformed in the frquency domain to CIE chromticity coordinates. The colour water-mark is then placed on top of the host image. Another methodology employs the quaternion Fourier transform for injecting a frequency domain water-mark after encoding the pieces of a color images.

The experimental data reveal that the imperceptibility is raised, and the robustness is greater over external attacks and multiple digital sig-nal processing techniques when compared to other existing systems. The method demonstrates that the water-mark's strength is the best. The DFT method has shown to be very resistant to translation in variations, along with geometric at-tacks.

2.12.3 Singular Value Decomposition

In mathematics, a singular value decomposition SVD is the combination of a real / complex matrix. This methodology generalises the eigen decomposetion of a symmetric matrix with non-negative eigenvalues to any m ,n matrix by extending the polar decomposition.In statistics and digital signal processing, the SVD trans-formation is commonly utilised.

In the RGB colour space, [76] suggested a method for image water-marking that is both robust and undetectable. The water-mark is embedded in singular values by this way. The water-mark may be retrieved using SVD on the blue channel of the host image. When compared to existing approaches, the new method was found to be more resilient among other things, over Gaussian noise, motion blur, salt-and-pepper noise, median filtering assaults, and JPEG compression attacks.

2.12.4 Discrete Wavelet Transform

One of advantages of DWT over Fourier transforms is the temporal resolution (i.e., DCT and DFT). By acquiring numerous data characteristics, like position in time and frequency, DWT becomes a more appealing research subject. Wavelets, are used to deconstruct the signal. Digital signal processing, image compression, and signal noise reduction can all benefit from the wavelet transform.

In digital signal processeng, image compression, and signal noise reduction, the wavelet transform can be utilised. A wavelet transform's core concept is to em-ploy a set of fundamental functions. (called wavelets) to provide frequency domain localization. High frequency resolution could well be achieved at low frequencies using a wavelet transform, whereas high time resolution can be obtained at high frequencies [77].

The DWT image water-marking algorithm converts the initial image into three layers.. The water-mark is implanted at 3 independent layers and use the subbands . Sub-bands cover a large span of the image's frequency spectrum. As a result, the water-marking system's robustness is improved [78]. Figure below depicts a three-level DWT. When you've finished with the DWT, you can move on to the next step, that system uses an algorithm to embed the water-mark into to the cover image, then extracts the water-marked image using the inverse DWT. In the watarmark extraction procedure, the DWT is applied at the very same level to the water-marked image.. Finally, IDWT is used to create watermark image. The figure2.8 depicts the entire procedure.

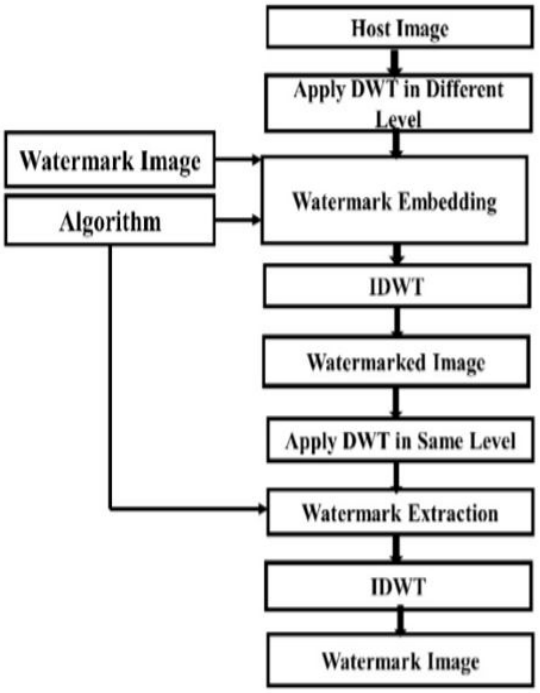

FIGURE 2.8: Discrete wavelet transform [78]

In an other study [79], the watermark was extracted without the need for the actual host / watermark image. With one-level DWT performed to every element of the cover image, a colour image watarmarking method that based on Discrete Wavelet Transform and quick response decomposition was presented. The colored candidate image is segmented into four nonover-lapping sections, with QR

decomposition applied to each pixel block. By measuring the first-row elements of the matrix R, the watermark can be inserted this way. The suggested method is more robust to noise, image compression, cropping, and filtering than comparable existing methods.

2.12.5 Hybrid Domain Watermarking Algorithms

In the hybrid domain, watermarking methods are often a mix of spatial and transform-domain algorithms.These techniques provide increased data embedding qualities as well as increased robustness. The use of hybrid domain approacheshas been the subject of numerous studies. The latest trends in watermarking are reflected in these studies.

Authors of refer, for example, [80] integrated the spa-tial and frequency domains for image watermarking, enabling for more watermark data to be implanted in the host image.The spatial domain replaces the host im-age's LSB bits with the watermark image's bits. By expanding the host image's capacity and separating the watermark into two pieces, this methodology twice the defense.To boost robustness against signal processing assaults like image crop-ping, a random permutation of the watermark might be used.

A new mechanism [81] was devised to defend digital rights in a hybrid domain. The method protects electronic information while communication over a non-secure medium while using the least significant bits and a wavelet transform (DWT and SVD), in which the host image is divided into sub-bands using a frequency domaintransformation mechanism. The watermark is extracted through using embedding processes that were previously established. This hybrid approach is more resilient such as Gaussian noise and JPEG compression, and has a greater quality.A further study employed DCT and DWT to improve the robustness of the water-marking system[82].

The watermarking service's robustness and imperceptibility are provided via ahybrid technique of DWT and SVD [83]. Existing watermarking techniques areless robust to geometric attacks. Like a result, to withstand geometric assaults, amulti-watermarking strategy based on dual-tree complex wavelet transform, DCT,and a Henon Map has been created for medical image [60]. This technique canhelp with medical security, secure authentication, cloud storage, and cloud trans-mission.

2.13 Attacks on Watermarked Image

There are four types of attacks under the broad category of existing attacks: re-moval attacks, geometric attacks, cryptographic attacks, and protocol attack[84].

2.13.1 Removal Attacks

The goal of a removal attack is to completely remove the watermark informationfrom the watermarked material without compromising the security of the watermarking technique (for example, by removing the key used for watermark embedding).Denoising, quantization (for example, for compression), remodulation, and collusion attacks all fall within this area. Although not all of these approaches achieve their goal of total watermark elimination, they may cause significant damage to the watermark information[84].

2.13.2 Geometric Attacks

Geometric attacks, in contrast to removal attacks, aim to corrupt the watermarkdetector's synchronisation with the embedded information rather than actually removing the embedded watermark.When perfect synchronisation is restored, the detector may be able to recover the imbedded watermark information.However, the needed synchronisation mechanism may be too complicated to be feasible.[84].

2.13.3 Cryptographic Attacks

Cryptographic attacks try to break the security measures used in watermarkingschemes, allowing the embedded watermark information to be removed or fake watermarks to be placed.The brute-force search for embedded secret information is one such strategy.When a watermark detector device is present,another attack in this category is also the Oracle attack, which can be used to create a non-watarmarked signal,because of their great computing complexity,these at-tacks are limited in their practical application.The publication [85] described and analysed many methods of attacks on digital image watermarks.Salt-Pepper noise,Gaussian noise, and Histogram-Equalization attacks are examples of attacks.

They conclude from their findings that existing approaches have varying degrees of sensitivity and resistance to various threats.In their experiment, they show that neither the LSB nor the DWT approaches have a clear edge over one another in terms of resistance to these attacks. This study [86] proposes a QR-based digital watermarking approach for cropping attack resistance. The primary goal of this research was to improve the robustness against cropping attacks; As a result, they didn't place a premium on image processing robustness. The variable K was employed to achieve a balance between imperceptibility and robustness in this study. he R matrix's four elements were all given the identical K value. Setting varied K values for distinct concealed places can actually improve imperceptibility and robustness.

Chapter 3

Fundamentals of Watermarking Techniques

The basics and structure of Hessenberg Decomposition ,Discrete wavelet transform and singular value decomposition are covered in this chapter.

3.1 Hessenberg Decomposition

Hessenberg Decomposition is a kind of matrix decomposition that may be applied to square matrices [87]. A mxm matrix can be divided using HD as

$$\mathrm{PHP}^{\top} = \mathrm{HD(Y)} \tag{3.1}$$

Where P is an orthogonal matrix and H is an uper Hessenberg matrix, h and j=0.The Householder matrices are commonly used to compute HD. The Householder matrix is an orthogonal matrix with the formula

$$\mathrm{Q} = \left(\mathrm{I_n} - 2\mu\mu^{T}\right) / \mu^{T}\mu \tag{3.2}$$

where μ is a nonzero vactor i mxm identity matrix. The whole technique consists of m stages. As a result, HD is calculated as

$$P = \big(Q_1 Q_2 \dots Q_{n)} \times (Q_1 Q_2 \dots Q_n) \tag{3.3}$$

$$H = P^{\top} Y P \tag{3.4}$$

$$Y = PHP^{T} \tag{3.5}$$

HD can find a more accurate component of the candidate image, which increases the robustness[88].

3.2 Discrete Wave Transformation

The discrete wavelet transform (DWT) is a very well technique with several uses in engineering and science.[89] It gives an energy-efficient representationof the image and has a positive impact on image analysis attack resistance in watarmarking.[90].Discrete wavelet transform divides the candidate image into subbands: low high (LH), high low (HL), high high (HH), and low low (LL).After one level of Discrete wavelet transform, the volume of data in the candidate image is contained in the LL subband.The wavelet model allows for further subdivision till the size of the sub bands meets the watermark requirement.

When compared to other subbands,subband LL performs better on attacks such as filter and com-pression attacks. [91].The LL subband is a good choice for robust watermarking because of this property[92].

3.3 Singular Value Decomposition

Singular values are separated in the form of diagonal matrices when SVD breaks down a symmetric matrix into three submatrices[93]. Left singular matrix U,

singular matrix S, and right singular matrix V are the three decomposed matrices when the matrix diagonalization is applied.If X is a symmetric matrix, then SVD can be calculated as follows:

$$\mathrm{ABC}^{\top} = \mathrm{SVD(X)} \tag{3.6}$$

A contains orthonormal eigenvectors, B contains orthonormal eigenvectors, and C contains the square roots of the eigenvalues from A or C in descending order. In this study, the SVD singular value B is used, and the watermark's singular value is embedded into the host picture using a suitable scaling factor.

Chapter 4

Proposed Research Technique

4.1 Introduction

This section proposes a technique to segment and watermark BrainWeb MRI with different Noise and INU levels mainly this section consist of segmentation and watermarking. Image segmentation consist of preprocessing, training network and segmentation described below while Image watermarking presented below in this chapter as S the watermarking embedding methodology, watermarking extraction methodology. In addition, different attacks also performed to check robustness and imperceptibility.

This chapter goes through each phase of the proposed technique in detail. The chapter also includes a description of the dataset as well as the experimental setup. whereas Figure below depicts the proposed technique's scheme.

1. **Pre-processing**

   Preprocessing is a data mining approach that requires converting a dataset into a format that is understandable to the user. Noise removal, contrast, and the dimension of the image are adjusted. Skull stripping (the removal of the outer ring of the brain picture) is also done. soft-tissues of the brain MR images are the output of this stage.

2. **K-means**

   In this stage, the K-means clustering method is used to label a skull-stripped brain MR image that only contains soft tissues.

3. **ANN**

   A feedforward-back propagation ANN network is trained in default settings on the labeled data that was obtained by K-means, to accurately segment brain MRI into distinct types of soft tissues, such as WM, GM, and CSF.

4. **Waterrmarking**

   The suggested watermarking approach will employ DWT, HD, and SVD on the each segments to watermark them and finally differents attacks will be performed to ensure invisibility and robustness.

5. **Performance Measures**

   Different performance metrics including PSNR, SSIM, NC, and STD are measured to ensure the accuracy of our results.

4.2 Dataset Acquisition

Images involved in this experiment for segmentation and watermarking come fromthe domain of health sector. Brain images are selected as the host image and ran-dom png images are selected as logo image. Medical images hold decisive property and are very crucial and important part of medical information. Therefore, it is very much important to secure these images by such techniques which can resist various attacks.

4.2.1 Selection of Host Image[1]

As the host picture, brain images from the Simulated Brain Database were em-ployed. The SBD contains a collection of real MRI large datasets produced by an

[1]https://brainweb.bic.mni.mcgill.ca/cgi/brainweb1

MRI simulator. In a circumstance when the truth was revealed, the neuroimaging community can use these data/information to monitor the effectiveness of different image analysis tools. Simulated brain MRI images for 2 anatomical models normal and multiple sclerosis, is presently available in the SBD . Three series (T1-, T2-, and proton-density- weighted) and also a range of layer depths, noise levels, and intensity non-uniformity levels were used to mimic full 3-dimensional data volumes for both of these. Brain images selected as host image with different noise level are shown below

TABLE 4.1: Description of data set

Images	Noise- Level (%)	INU-Level (%)
Case-0	0	0% 20% 40%
Case-1	1	0% 20% 40%
Case-3	3	0% 20% 40%
Case-5	5	0% 20% 40%
Case-7	7	0% 20% 40%
Case-9	9	0% 20% 40%

4.2.2 Watermark Image

We have used test image cameraman.tif as watermark shown in figure 4.1.

FIGURE 4.1: Watermark image

4.2.3 Programming Language

Mathworks produced MATLAB, a multi-paradigm programming language and numeric computing environment. Matrix operations, function and data visualisation, technique development, ui building, and connecting with programmes written in other languages are all available with MATLAB.

4.2.4 Tools Used

The tool used for the implementation is MATLA.

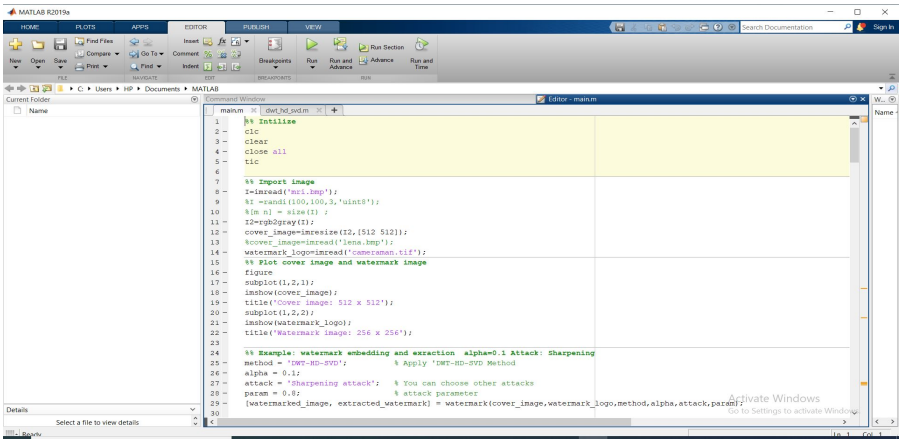

FIGURE 4.2: Frontend of matlab

Thousands of researchers and technicians use MATLAB to analyse data, develop new methods, and build models.

4.2.5 Machine Configuration

The project was completed on an HP i5 machine.

Processor/CPU: Intel Core i5-5200U (5th Generation, 3M Cache, up to 2.70 GHz)

Windows 10 Pro is the operating system.

4.3 Proposed Methodology Steps

Step 1: Retrieve images from the database.

Step 2: Perform pre-processing of images e.g., noise removal, contrast adjustment, dimensions fine-tuning, and skull stripe that is the exclusion of the outer

ring of the brain MRI.

Step 3: After obtaining the requisite images that are the soft tissues only and provide them to the K-means clustering algorithm for labeling the image.

Step 4: LM algorithm is applied for training and simulating the ANN network with this labeled data.

Step 5: After training the network , test data is provided to ANN and segmentation output is generated by ANN.

Step 6: The segmented contents generated by ANN are then watermarked by dwt-hd-svd.

Step 7: Finally, the watermarked images are evaluated by using different evaluation metrices.

Architecture diagram is shown in figure 4.3.

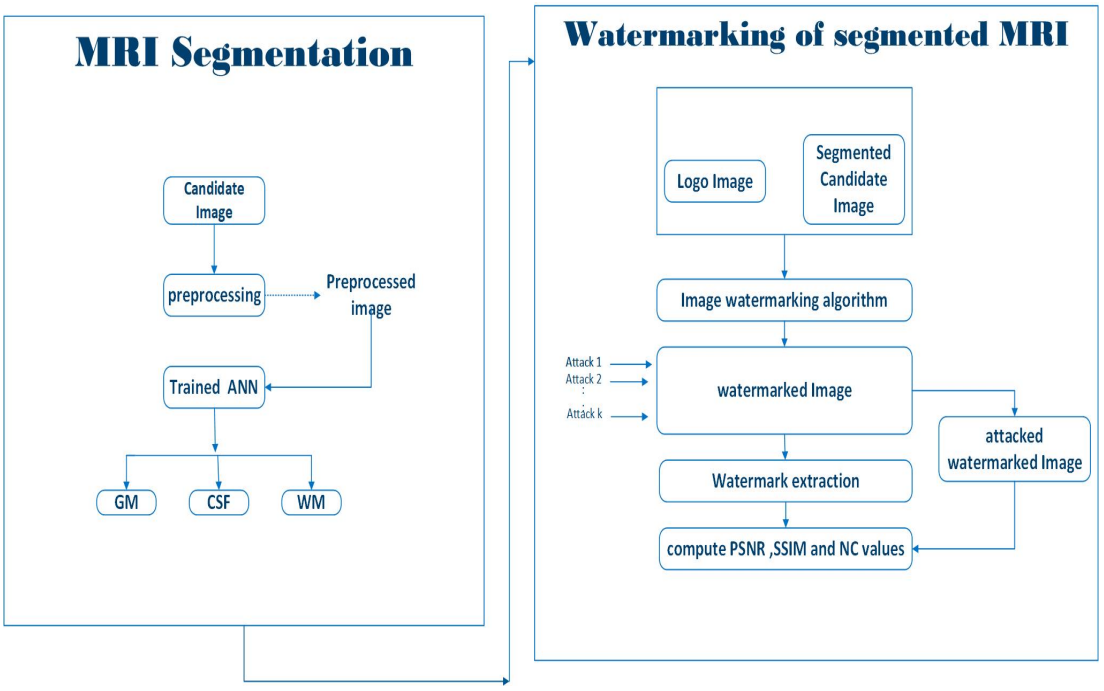

FIGURE 4.3: Architecture diagram

The architecture diagram shows the flow of the proposed technique. In the first step, Brain MRI is passed to ANN based segmentation algorithm Leven Berg which segment image into GM, BM and WM. After segmentation each segmented part is watermarked by using watermarking algorithm. Then different attacks are performed to check invisibility and robustness PSNR, SSIM and NC values are computed.

4.4 Image Segmentation

For Image segmentation ANN is trained in default setting by Leven berg. Leven berg's ANN-based image segmentation technique.It is also referred as the damped least-squares approach. In least squares curve fitting, these minimization concerns are especially prominent. The LMA can be used in many software applications to tackle general curve-fitting difficulties. The LMA, like other fitting techniques, merely finds a local minimum, that might or might not be the global minimum. Between both the Gauss–Newton algorithm and the gradient descent methodology, the LMA helps bridge the gap. Since the LMA is much more resilient than that of the GNA, it really can frequently discover an answer even though it starts from a very low point. For very well functions and appropriate beginning values, the LMA is slower than the GNA. Architecture diagram of image segmentation is shown in figure 4.4.

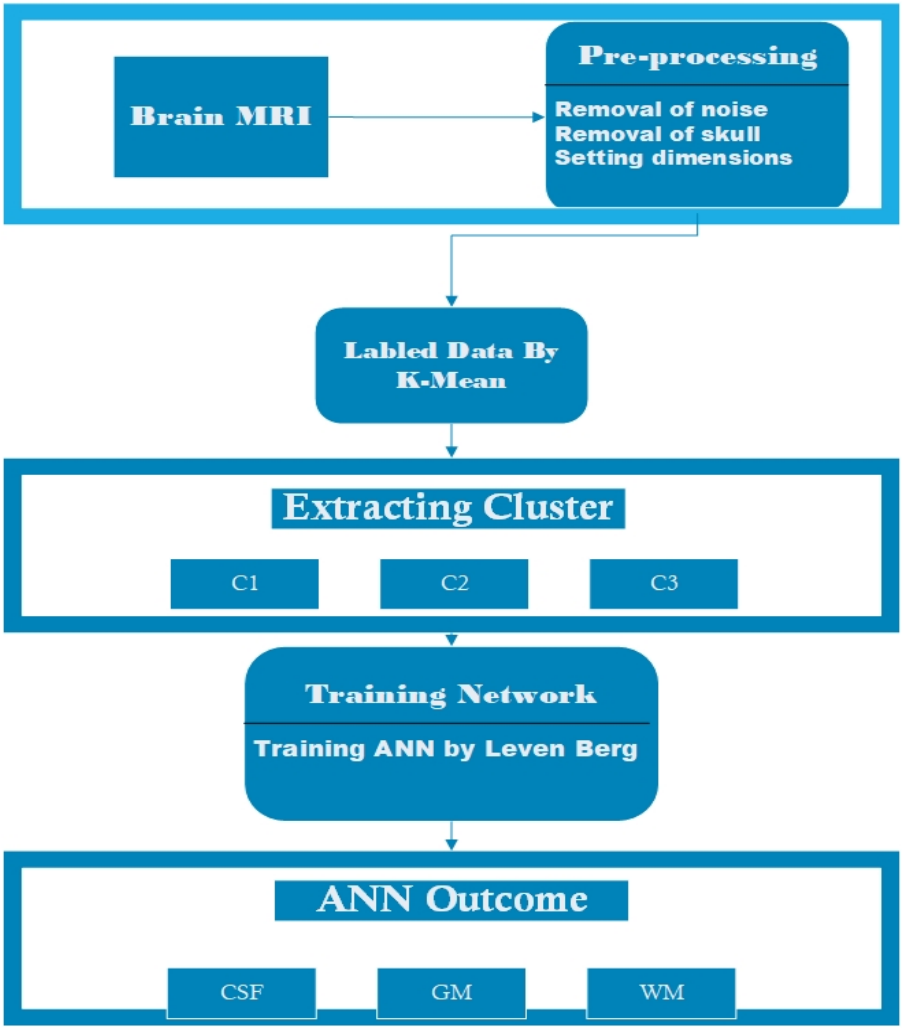

FIGURE 4.4: Architecture diagram

Image segmentation based on three steps Preprocessing, Train network and Segmentation. In first step brain image is converted into skull free image.it takes brain image as input and get the total number of rows and columns and,mostimportantly, the number of color channels to convert it into gray scale.Then extract 2 largest blobs, which will either be the skull and brain and fill any holesand region in the brain by (BW, locations) Dilate mask out a bit in case we've chopped out a little bit of brain. After that Mask out the skull from the original gray scale image to make it skull free image. Next step after preprocessing is totrain network. network is trained by reading training data and save information in 100X100 array .it first reads GM clusters ,then reads WM clusters and then reads CSF clusters. After training network next step is to segment preprocessed skull free image into white matter, gray matter and CSF by trained network and after that load trained network and take preprocessed image a input and resize it ,reshape input image and Segment input image into CSF , gray and white matter.

Pseudocode of image segmentation is presented below

TABLE 4.2: Pseudocode of image segmentation

Pseudocode
1. for all training images in the database do
2. input: images
3. preprocessing: remove noise, set contrast, set dimensions
4. skull stripe the images
5. apply k-means to get labeled data for each input image I
6. end for
7. for all labeled data do
8. train ANN by default setting
9. end for
10. for all images, Tn do
12. output: get a segmented image for each test image T

4.5 K-means Clustering and its Pseudocode

K-Mean is one of the most frequently and straightforward unsupervised-learning methods. This is a hard clustering method [94], which means that each data point belongs to just one cluster.K-Mean determines centroids at random for data processing, these cluster centers are the starting locations, and the optimum places are found through iterations. As noted in step 1 begins by working with a set of data items and the number of required clusters (K) [94].It starts by selecting centroids at random from the data elements for each cluster "K."Calculate the gap in between identified datasets and the rest of the items todetermined to see if the initial centroids' estimation was correct or not [95].And allocates the data element to the cluster with the shortest distance between them. It recalculates the centroids by taking the arithmetic mean of each cluster's data elements and reassigning the data elements to the cluster with the shortest dis-tance between the data element and the cluster's centroid repeated the steps until reaching the convergence [96].

4.5.1 Pseudocode of K-means

Step 1: INPUT : Array [97] be the set of input data points and k, number of desired clusters[98, 99].

Step :2 Initialize: Cluster centroids $C\{c_1, c_2, c_3...c_k\} \epsilon R_m$ randomly.

Step 3: For every $a_i \epsilon$ 1, . . . , n, set, c_i=argmin j ϵ 1, . . . ,k, $\|a_i - C_j\|^2$

$$C_j = \frac{\sum_{i=1}^{n} 1\{C_i = j\} x_i}{\sum_{i=1}^{n} 1\{C_i = j\}} \tag{4.1}$$

Step:5 Repeat steps 3 and 4 as needed to reach the maximum number of iterations or until the centroids do not change anymore.

Step :6 Output: Clusters $C\{c_1, c_2, c_3...c_k\}$.

4.6 Steps of ANN [100, 101]

The following fundamental steps are commonly computed by an ANN with back-propagation.

Step 1: Set the weights and biases to their initial values.

Step 2: For each input layer unit 'q', propagate the input forward.

Step 3: For any hidden or output layer unit 'q,' the output 'Outq' of an input unit 'q' is its real input value 'Inpq,' as Outq = Inpq.

Step 4: To propagate the input forward, compute the net input of unit 'q' concerning the preceding layer 'p' as Inpq = P $\sum \omega_{qp} out_p + \gamma_q$, where '$\omega_{qp}$' is the weight of the connection from unit 'p' in the preceding layer to unit 'q'.'Outp' is the output of unit 'p' from the preceding layers and 'γ_q' represents the bias of the unit.

Step 5: Analyse each 'q' unit's output as $Out_q = \frac{1}{1+\beta^{-1}q}$.

4.7 Image Watermarking

The suggested watermarking approach will employ DWT, HD, and SVD. Under robustness attacks, DWT's time-scale signal multi-resolution can increase watermarking performance. Meanwhile, when HD is used as the matrix transform, the resilience improves even more. Furthermore, when countering geometric attacks, the SVD-based watermarking method performs better. Finally, Different attacks are performed on watermarked images to check robustness and imperceptibility by calculating NC and PSNR values .Image watermarking based on two steps wa-termarking embedding and watermarking extraction.

4.7.1 Watermarking Embedding Process

The embedding procedure requires two inputs the candidate image A as well as the watermark B, and outputs the watermarked candidate image A*. The related

sizes of A, B, and A* are X into X, Y into Y, and X into X.The candidate image isreconstructed using Rlevel Discrete wavelet transform, a watermarking technology that can accommodate watermarks of various sizes. The embedding strategy for watermarking is represented in the diagram below, and the exactprocedures of embedding are explained in the stages that follow. Figure 4.5 shows an architecture diagram of the watermarking embedding procedure. 4.5

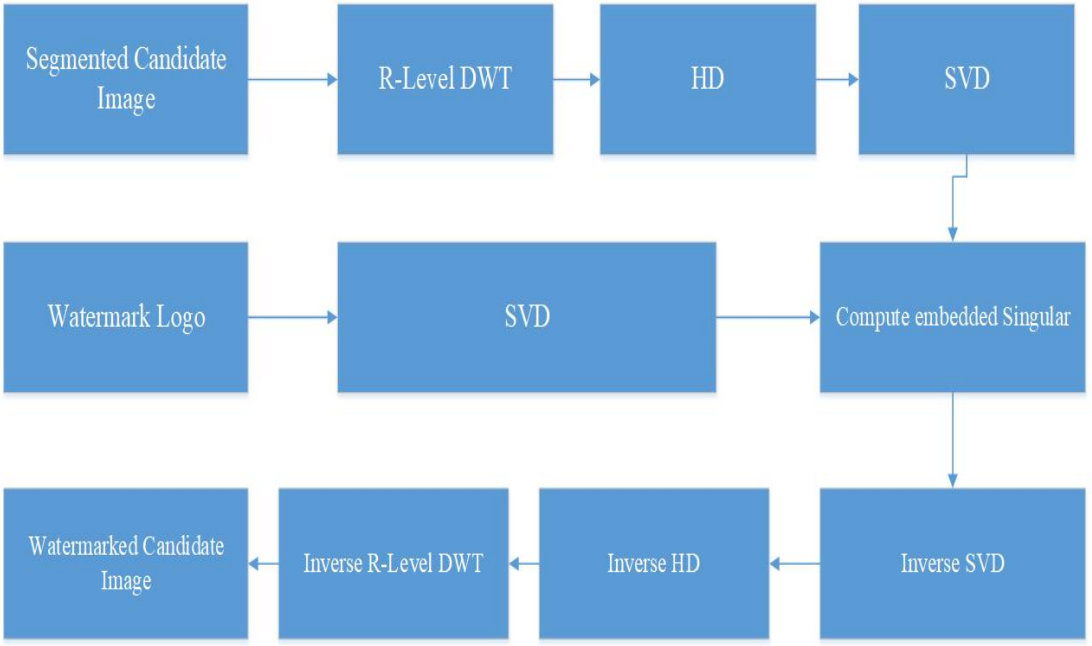

FIGURE 4.5: Watermarking embedding process

A is divided into LL, LH, HL, and HH components using Rlevel Discrete wavelet transform, with Result=log2 X/Y.

At first applied Rlevel Haar wavelet and decompose image into subbands ,then applied Hessenberg matrix ,when R is equal to 1 Applied 1-level Haar wavelet and ,apply Hessenberg matrix ,when R is equal to 2 Apply 1-level Haar wavelet and apply 2-level Haar wavelet on LL sub-band ,HD is performed on LL2, after that apply SVD to H matrix also applied SVD to watermark B and then embedded singular value is Computed with a scaling factor alpha 0.05 .The inverse of SVD is used to calculate the watarmarked subband. Based on the inverse of HD, a new low frequency approximation subband LL is reconstructed. Finally, the watermarked image is created using the 1-level inverse DWT.

TABLE 4.3: Pseudocode of watermarking embedding process

Pseudocode
Input: Candidate image; Watermark
Output: watermarked host image
1: Apply R-level Haar wavelet and decompose image into sub-bands
2: Apply Hessenberg matrix
3: Apply SVD to H matrix
4: Apply SVD to watermark logo
5: Compute an embedded singular value
6: Generate watermarked sub-band by using the inverse SVD
7: Obtained watermarked image by performing the inverse R-level DWT

4.7.2 Watermarking Extraction Process

The watermark that extracted A is the output of the watermarking extraction procedure, while the watermarked host picture B* is the input. The size of A is NbyN. The extraction of watermark approach has been seen in figure 4.6, and the exact extraction techniques are as follows.

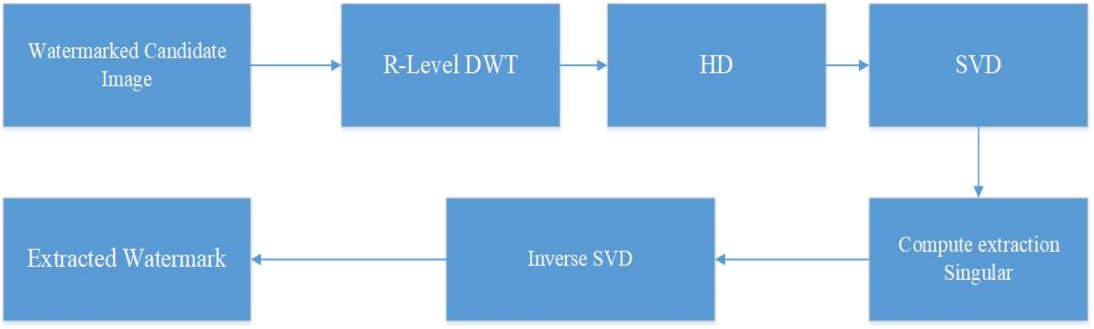

FIGURE 4.6: Watermarking extraction process

R level DWT decomposes the watermarked host picture B into subbands. and then HD is performed on Lowest frequency after that applied SVD to H.The extracted singular value is calculated by subtracting left-singular matrix from right-singular matrix and dividing by alpha 0.05.Finally the extracted watermark is

reconstructed by inverse SVD

TABLE 4.4: Pseudocode of watermarking extraction process

Pseudocode
Input: Watermarked Candidate Image
Output: Extracted Watermark
1: Decompose watermarked host image by R-level DWT
2: Apply HD on LLw
3: Apply SVD to Hw
4: Apply SVD to watermark logo
5: Compute extraction singular value
6: Apply inverse SVD
7: Obtained extracted watermark

4.8 Evaluation Metrices

To check the accuracy for results different performance matrices such as dice similarity coefficient (DSC), Mean Square Error (MSE), peak signal-to-noise ratio (PSNR),structural similarity index measure(SSIM)and Normalized correlation (NC) is calculated.

4.8.1 PSNR [102]

The peak signal-to-noise ratio is the ratio of an image's maximum achievable power to the power of damaging noise that influences its representation quality.

$$\mathrm{PSNR}\left(A, A^{*}\right) = 10 \lg \frac{A_{\max}^{2}}{\mathrm{MSE}} \tag{4.2}$$

$$\mathrm{MSE} = \frac{1}{X^{2}} \sum_{i=1}^{X} \sum_{j=1}^{X} \left(A_{i,j} - A_{i,j}^{*}\right)^{2} \tag{4.3}$$

where MSE is the mean square error between the candidate image and the watermarked candidate image, and Amax is the candidate image's maximum pixel value.

4.8.2 SSIM [102]

The Structural Similarity Index is a perceptual metric that measures image quality degradation as a result of processing such as data compression or data transmission losses.

$$\mathrm{SSIM}\left(A, A^{*}\right)=\frac{\mu_{A} \mu_{A^{*}}+d_{1}}{\mu_{A}^{2}+\mu_{A^{*}}^{2}+d_{1}} \cdot \frac{\sigma_{A A^{*}}+d_{2}}{\sigma_{A}^{2}+\sigma_{A^{*}}^{2}+d_{2}} \tag{4.4}$$

4.8.3 NC [102]

The robustness of the initial and extracted watermarks is commonly assessed using normalised correlation (NC), which is defined as

$$\mathrm{NC}=\frac{\sum_{i=1}^{X} \sum_{j=1}^{X} B_{i, j} B_{i, j}^{*}}{\sqrt{\sum_{i=1}^{Y} \sum_{j=1}^{Y} B_{i, j}^{2}} \sqrt{\sum_{i=1}^{Y} \sum_{j=1}^{Y} B_{i, j}^{* 2}}} \tag{4.5}$$

4.8.4 DSC

The dice similarity coefficient (DSC) is amongst the most widely used evaluation metrics in medical image segmentation. The DSC value is a straightforward and practical description of spatial overlap that may be used to improve image segmentation accuracy. A DSC has a value between 0 and 1, with 0 indicating no spatial overlap and 1 representing the total overlap between two sets of binary segmentation results. The DSC is defined as a measurement of the spatial overlap across two segmentations, A and B target regions.

$$DSC=(A, B)=2(A \cap B) /(A+B) \tag{4.6}$$

Where A is the specific region in segmented output and B is the same region in GT image, ∩ is the intersection of a specific region of A and B.

4.8.5 MSE

Mean Squared Error (MSE) can be defined as the average of the squares of the errors obtained by subtracting the segmented output and GT image values. It can be defined as the average square of the errors obtained by subtracting the segmented output and GT image values. It can be expressed as

$$MSE = \frac{1}{mn} \sum_{i=0}^{m} \sum_{j=0}^{n} [R(i,j) - S(i,j)]^2 \tag{4.7}$$

Where, 'R(i,j)' represents the reference image and 'S(i,j)' represents the segmented image. 'm' represents the number of rows and 'n' represents the number of columns in segmented images and reference image. 'i= m' denotes the row-wise increment and 'j = n' denotes the column-wise increment in for loop. The MSE value for the resulting segmented image should be as lowest as possible. Reduced MSE values give a reduced occurrence of an error in segmented images.

4.9 Trade-off between Invisibility and Robustness

Invisibility is often determined using perfrmance measurments such as the maximum signal to noise ratio. The structural similarity index and PSNR are two noise metrics (SSIM). It is characterised by

$$\text{PSNR}(\dot{j}, \dot{i}) = \text{ psnr (watermarked image, cover image)} \tag{4.8}$$

SSIM compares the similarity of watermarked image and original image

$$\text{SSIM}\,(jhi) = \text{ ssim(watermarked image, cover image)} \tag{4.9}$$

Where as i represent attack and j represent alpha values ,The resilience of the original and extracted watermarks is frequently assessed using normalised correlation (NC), which is defined by

$$\mathrm{NC}\,(js) = \mathrm{nc}\ (\text{watermark logo, extracted watermark}) \tag{4.10}$$

4.10 Attacks on Watermarked Image

The watermarked candidate image is subjected to a number of attacks, including a Gaussian-low-pass filter, Median, Gaussian-noise, Salt-Pepper-noise, and others. Noise in the form of speckles 'Sharpening attack,Histogram equalisation' Average filter,Motion blur with varying watermark sizes' Rotating attack,Crop attack,JPEG compression,JPEG2000 compression,'Sharpening attack,Histogram equalisation'

Table 4.5: Attacks and specifications

Attacks	**Specifications**
Median Filter	(3 x 3)
Gussian low-pass Filter	(3 x 3)
Averaige Filter	(3 x 3)
Gussian noise	0.001
Salt and pepper noise	0.001
Speckle noise	0.001
Cropping attack	2 percent
JPG Compression	QF=50
JPG2000 Compression	CR=12
Rotation atatck	2 Degree
Motion Blur	theta=4 ,len=7
Sharpening attack	0.8

The parametars in the above test attacks are fixed, but dynamical parametars should be examined as well to better illustrate the robustness of the suggested technique. The experiments with different parameters are carried out and tested, with the results presented in the following chapter.

Chapter 5

Results and Discussion

This chapter provides discussion on the experiment and results achieved by the methodology discussed in the previous chapter.At first the segmented results of brain MR images obtained by each step of the methodology. Such as preprocessing in which colored images are converted into grayscale images, dimensions, and skull stripping of the images performed. Then the soft tissues are provided to the clustering algorithm for labeling. After that, the labeled data is trained on ANN network and tested to perform the accurate segmentation of brain MRI into different types of soft tissues e.g., WM, GM, and CSF.

The invisibility and robustness of the suggested watermarking approach for segmented brain images with different noise and inu are examined in this section. Segmented brain images with different noise level and INU is also discussed in this section below.

Subjective eye observation and objective quantitative analysis are used to detect the suggested method's invisibility and resilience. Furthermore, a variety of assaults with varying parameters are employed to test the robustness of the system. The software used is MATLAB R2019a. In the experiments, the segmented host images of brain with various noise and INU level also are presented below.Image of "cameraman.tiff" of 256x256, 128x128, and 64x64 are used as watermark images and are shown below Various attacks are performed to test the robustnes.

Images with watermarks are vulnerable to attacks.Filter,noise, cropping, compression, rescaling, histogram equalisation (HE), motion blur, sharpening, and rotation attacks are among the attacks.

5.1 Segmentation of Images

segmentation results generated by ANN using the 'lm' algorithm for the test image can be shown in Figure below Segments of image with 0 percent Noise and 0 percent INU presented in figure5.1.

(a) (b) (c)

FIGURE 5.1: (a) CSF (b) GM (c)WM

Segments of image with 0 percent Noise and 20 Percent are INU presented in figure5.2.

(a) (b) (c)

FIGURE 5.2: (a) CSF (b) GM (c)WM

Segments of image with 0 percent Noise and 40 Percent INU presented in figure 5.3.

(a) (b) (c)

FIGURE 5.3: (a) CSF (b) GM (c)WM

Segments of image with 1 percent Noise and 0 Percent INU presented in figure 5.4.

(a) (b) (c)

FIGURE 5.4: (a) CSF (b) GM (c)WM

Segments of image with 1 percent Noise and 20 Percent INU presented in figure 5.5.

(a) (b) (c)

FIGURE 5.5: (a) CSF (b) GM (c)WM

Segments of image with 1 percent Noise and 40 Percent INU presented in figure 5.6.

(a) (b) (c)

FIGURE 5.6: (a) CSF (b) GM (c)WM

Segments of image with 3 percent Noise and 0 Percent INU presented in figure 5.7.

(a) (b) (c)

FIGURE 5.7: (a) CSF (b) GM (c)WM

Segments of image with 3 percent Noise and 20 Percent INU presented in figure 5.8.

(a) (b) (c)

FIGURE 5.8: (a) CSF (b) GM (c)WM

Segments of image with 3 percent Noise and 40 Percent INU presented in figure 5.9.

(a) (b) (c)

FIGURE 5.9: (a) CSF (b) GM (c)WM

Segments of image with 5 percent Noise and 0 Percent INU presented in figure 5.10.

(a) (b) (c)

FIGURE 5.10: (a) CSF (b) GM (c)WM

Segments of image with 5 percent Noise and 20 Percent INU presented in figure 5.11.

(a) (b) (c)

FIGURE 5.11: (a) CSF (b) GM (c)WM

Segments of image with 5 percent Noise and 40 Percent INU presented in figure 5.12.

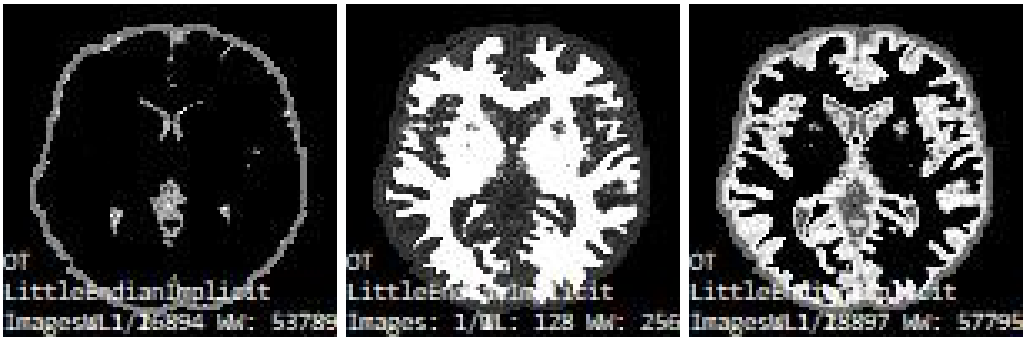

(a) (b) (c)

FIGURE 5.12: (a) CSF (b) GM (c)WM

5.2 Image Watermarking

After segmenting image into WM, GM and CSF each segmented part is watermarked by embedding watermark in host image using DWT-HD-SVD algorithm,The suggested watermarking approach will employ DWT, HD, and SVD. Under robustness attacks, DWT's time-scale signal multi-resolution can increase watermarking performance.

Meanwhile, when HD is used as the matrix trans-form, the resilience improves even more. Furthermore, when countering geometric attacks, the SVD-based watermarking method performs better.Finally,Different attacks are performed on watermarked images to check robust-ness and imperceptibility by calculating NC and PSNR values Image watermark-ing based on two steps watermarking embedding and watermarking extraction.So image watermarking includes three steps as follow

5.2.1 Embedding and Extracting Watermark

Results of watermark embedding and extraction of segments with 0 percent Noise and 0 **and** 1 percent INU level shown below in figure 5.13 **and** 5.14

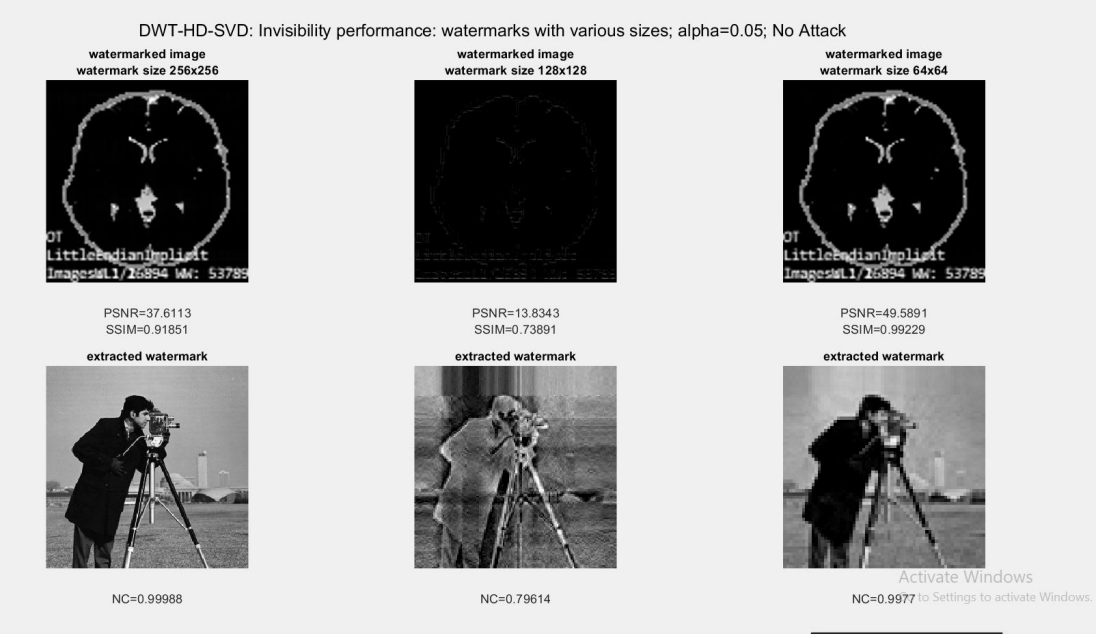

FIGURE 5.13: 0 percent noise and 0 percent inu

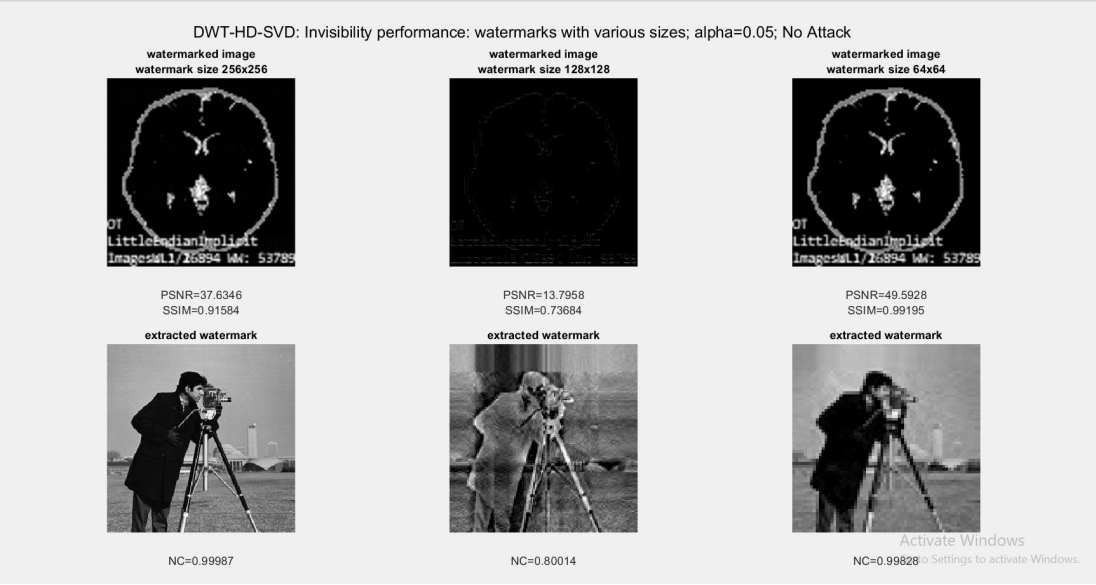

FIGURE 5.14: 0 percent noise and 1 percent inu

Results of watermark embedding and extraction of segments with 0 percent Noise and 3 and 5 percent INU level shown below in figure 5.15 and 5.16

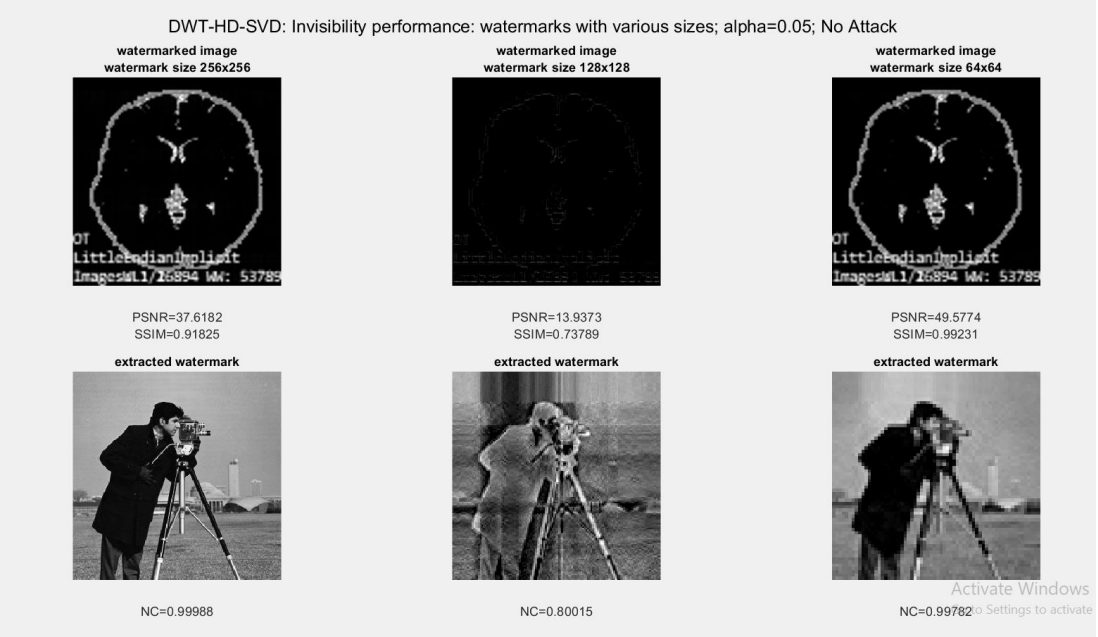

FIGURE 5.15: 0 percent noise and 3 percent inu

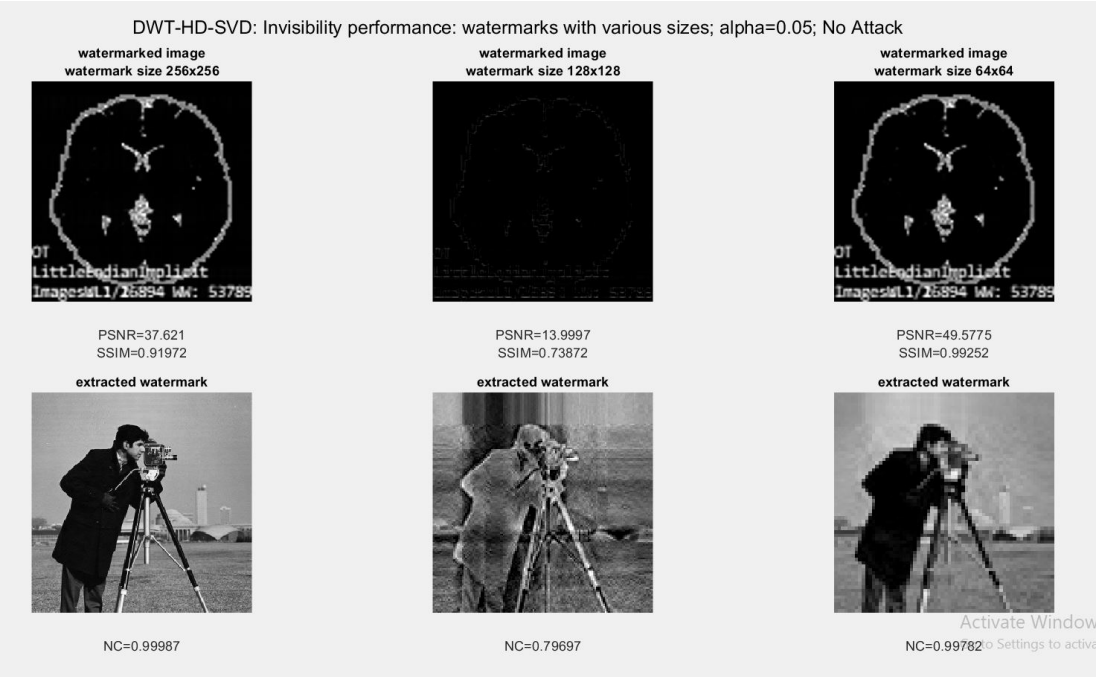

FIGURE 5.16: 0 Percent noise and 5 percent inu

5.2.2 Different Attacks and Specifications

Different attacks used in the experiments

TABLE 5.1: Attacks and specifications

Attacks	**Specifications**
Median Filter	(3 x 3)
Gussian low-pass Filter	(3 x 3)
Averaige Filter	(3 x 3)
Gussian noise	0.001
Salt and pepper noise	0.001
Speckle noise	0.001
Cropping attack	2 percent
JPG Compression	QF=50
JPG2000 Compression	CR=12
Rotation atatck	2 Degree
Motion Blur	theta=4 ,len=7
Sharpening attack	0.8

The parameters in the above test attacks are fixed, however dynamical parameters should be examined as well to better illustrate the robustness of the suggested technique.The experiments with different parameters are carried out and evaluated, with the findings given below.The robustness is evaluated using JPEG compression with various QFs ranging from 90 to 10 with a step of 10, where QF denotes compression strength. The image is compressed considerably when the QF is small.NC values are subjected to numerous attacks under different parameters. JPEG-compression, JPEG2000-compression, Gaussian -low-pass filter, median-filter, Gaussian-noise, and sharpening are all examples. JPEG2000 compression attack with CRs determined that larger the CR, the more compressed the image is

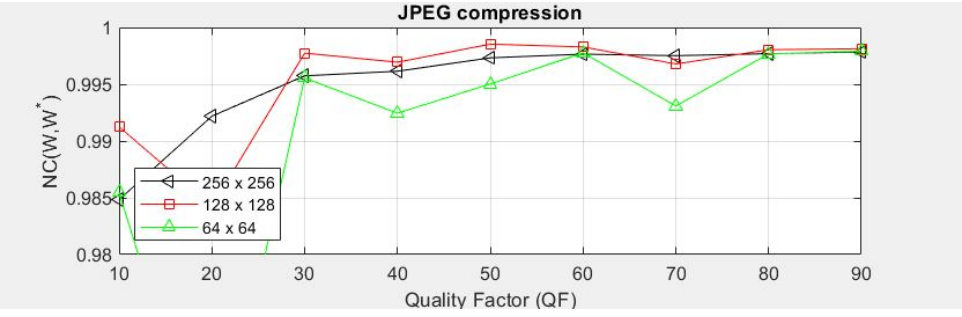

FIGURE 5.17: Robustness level with various parameters

Positive standard deviation sigma is set from 0.5 to 4.5 , and window size is set from 3X3 to 7X7 . NCs of Gaussian lowpass filters are all greater, according to the test results.

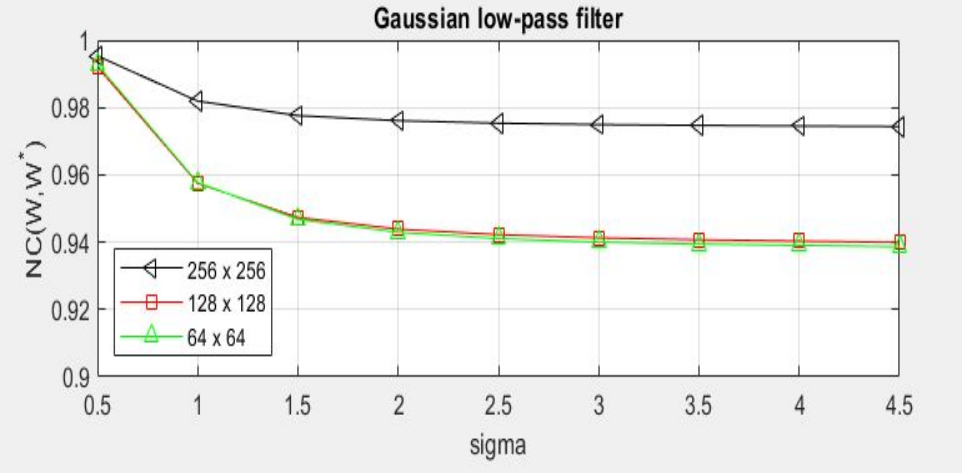

FIGURE 5.18: Robustness level with various parameters

For the watarmark size 64x64 and 256x256, the median-filter's NCs are all more than 0.91. The median attack's NCs also reach 0.95 for the 64X64 watarmark.

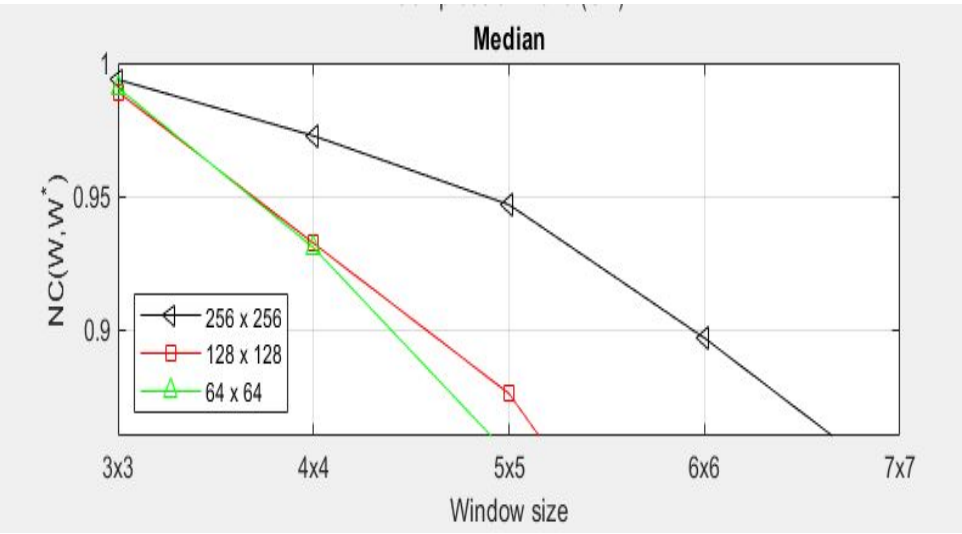

FIGURE 5.19: Robustness level with various parameters

The Gaussian-noise and sharpening are examined using different variance and threshold values, and the results are displayed below.Their setting ranges are [0.001,0.009]respectively.NCs of the Gaussian noise and sharpening are all larger than 0.8880 and 0.9880, respectively. Especially for 64X64 watermark, NCs for Gaussian noise and sharp-ening are all larger than 0.9500.

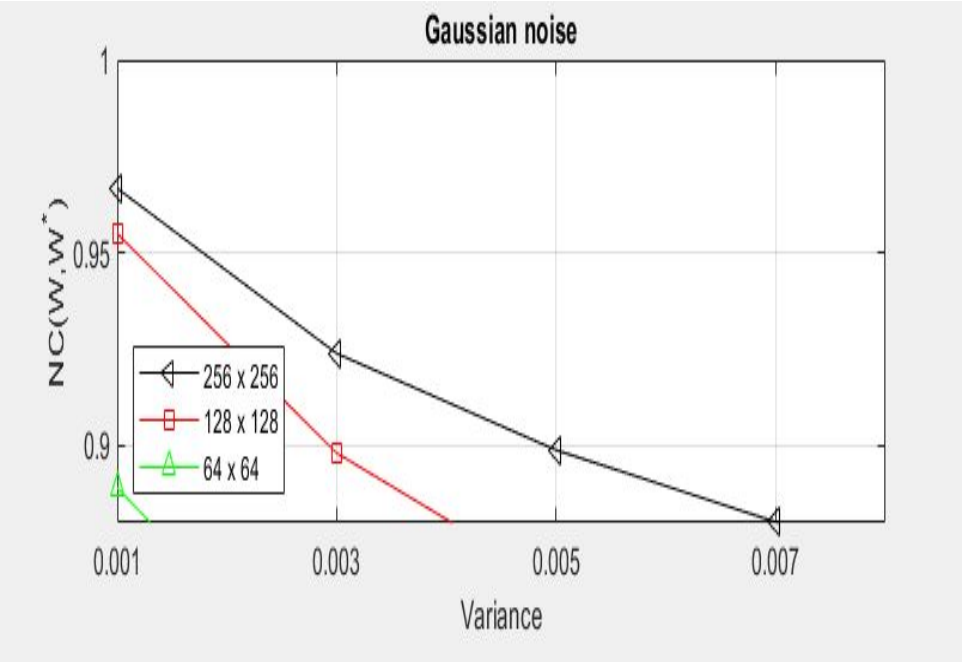

FIGURE 5.20: Robustness level with various parameters

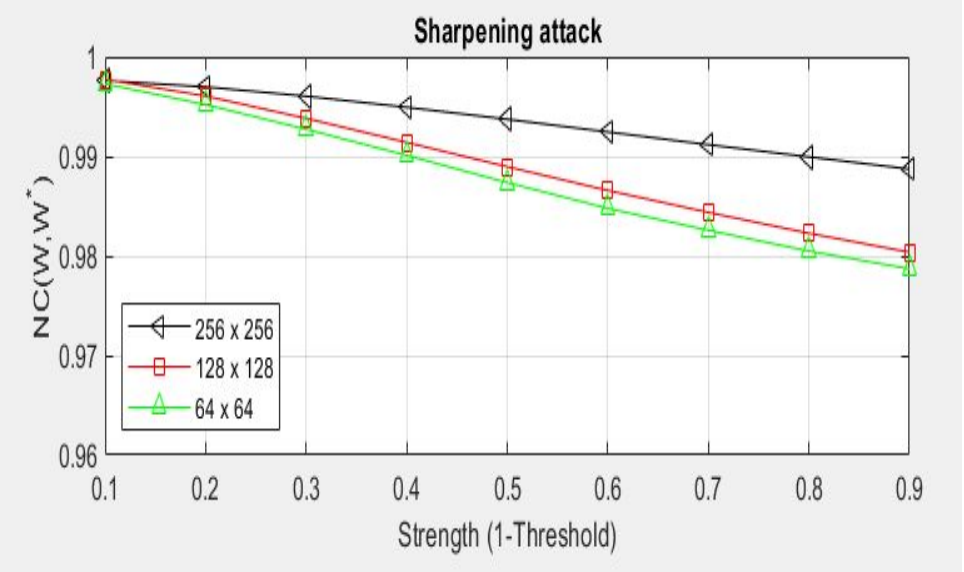

FIGURE 5.21: Robustness level with various parameters

The parameters in the above test attacks are static, and in order to further reflect the robustness of the proposed method, the case of dynamic parameters should be considered as well shown above.Results of using different parameter shows that level of robustness under different attacks increases while using parameters defined above.

5.3 Invisibility of Watermarked Image

To preserve the safety of information, the watermarked host image should be invisible to humans; thus, watermark invisibility is an important criterion to check performance.Tables below depicts PSNR values to check the invisibility watermarked segmented host images of MRI with 0,1,3 and 5 percent Noise and INU level that were attacked.

5.3.1 Peak Signal to Noise Ratio

Invisibility of attacked watermarked segment of 0-0-076 percent Noise and INU with watermark size 64X64

Table 5.2: Invisibility with size 64X64

Attacks	**CSF**	**GM**	**WM**	**RGB**
Median Filter	43.595	42.682	41.368	44.930
Gussian low-pass Filter	41.445	39.999	38.491	43.129
Averaige Filter	41.311	39.856	38.346	43.025
Gussian noise	32.063	31.349	31.403	30.779
Salt and pepper noise	32.788	33.682	33.815	34.462
Speckle noise	42.408	37.712	36.891	38.865
Cropping attack	10.535	6.0420	5.4760	10.754
JPG Compression	43.399	42.000	40.988	43.040
JPG2000 Compression	48.768	48.583	45.953	48.264
Rotation atatck	13.017	8.3480	7.3200	14.462
Motion Blur	32.108	30.876	29.421	34.380
HE	3.8080	10.869	9.1610	10.352
Sharpening attack	40.859	40.215	38.838	42.603

Invisibility of attacked watermarked segment of 0-0-076 percent Noise and INU with watermark size 128X128

Table 5.3: Invisibility with size 128X128

Attack	**CSF**	**GM**	**WM**	**RGB**
Median Filter	13.526	6.0800	6.6100	9.4220
Gussian low-pa-ss Filter	13.666	6.1360	6.6910	9.4760
Averaige Filter	13.666	6.1360	6.6910	9.4760
Gussian noise	13.734	6.2390	6.7800	9.6650
Salt and pepper noise	13.603	6.1280	6.6800	9.4650
Speckle noise	13.648	6.1310	6.6830	9.4730
Cropping attack	13.388	6.1230	6.6230	9.4520
JPG Compression	13.687	6.1440	6.7020	9.4750
JPG2000 Compression	13.661	6.1410	6.6970	9.4830
Rotation atatck	13.423	6.1070	6.6230	9.4180
Motion Blur	13.650	6.1330	6.6860	9.4720
HE	1.9020	4.8620	5.0050	4.8640
Sharpening attack	13.730	6.1650	6.7349	9.5100

Invisibility of attacked watermarked segment of 0-0-076 percent Noise and INU with watermark size 256X256

TABLE 5.4: Invisibility with size 256X256

Attacks	**CSF**	**GM**	**WM**	**RGB**
Median Filter	37.600	39.601	38.961	37.478
Gussian low-pass Filter	37.380	38.707	36.118	37.407
Averaige Filter	37.340	38.608	36.042	37.385
Gussian noise	30.822	31.005	30.618	30.025
Salt and pepper noise	31.638	32.856	32.007	32.437
Speckle noise	36.698	36.478	34.935	35.299
Cropping attack	10.368	6.028	5.420	10.598
JPG Compression	36.999	39.229	36.702	36.886
JPG2000 Compression	37.672	41.303	37.887	37.538
Rotation atatck	12.892	8.3500	7.2760	14.337
Motion Blur	31.610	30.737	29.136	33.240
HE	6.2510	11.055	11.213	10.658
Sharpening attack	35.298	37.451	35.151	36.059

Invisibility of attacked watermarked segment of 1-0-076 percent Noise and INU with watermark size 64X64

TABLE 5.5: Invisibility with size 64X64

Attacks	**CSF**	**GM**	**WM**	**RGB**
Median Filter	43.572	42.683	41.387	44.926
Gussian low-pass Filter	41.449	39.999	38.493	43.124
Averaige Filter	41.317	39.840	38.345	43.018
Gussian noise	32.030	31.315	31.417	30.765
Salt and pepper noise	33.607	33.872	33.102	34.248
Speckle noise	42.384	37.669	36.905	38.843
Cropping attack	10.867	6.0508	5.4424	10.723
JPG Compression	43.344	41.987	40.958	43.024
JPG2000 Compression	48.630	48.634	46.003	48.310
Rotation atatck	13.139	8.3490	7.3330	14.489
Motion Blur	32.092	30.863	29.407	34.368
HE	3.8050	10.877	9.1840	10.360
Sharpening attack	40.822	40.207	38.841	42.607

Invisibility of attacked watermarked segment of 1-0-076 percent Noise and INU with watermark size 128X128

TABLE 5.6: Invisibility with size 128X128

Attacks	**CSF**	**GM**	**WM**	**RGB**
Median Filter	13.671	6.0800	6.5970	9.4140
Gussian low-pass Filter	13.814	6.1400	6.6780	9.4680
Averaige Filter	13.814	6.1409	6.6780	9.4684
Gussian noise	13.885	6.2453	6.7682	9.6568
Salt and pepper noise	13.753	6.1326	6.6667	9.4540
Speckle noise	13.795	6.1359	6.6706	9.4657
Cropping attack	13.531	6.1275	6.6118	9.4441
JPG Compression	13.835	6.1429	6.7900	9.4673
JPG2000 Compression	13.809	6.1458	6.6970	9.4760
Rotation atatck	13.566	6.1114	6.6110	9.4104
Motion Blur	13.798	6.1375	6.6731	9.4646
HE	1.9040	4.8653	5.0133	4.8699
Sharpening attack	13.879	6.1697	6.7218	9.5021

Invisibility of attacked watermarked segment of 1-0-076 percent Noise and INU with watermark size 256X256

TABLE 5.7: Invisibility with size 256X256

Attack	**CSF**	**GM**	**WM**	**RGB**
Median Filter	37.458	39.614	38.957	37.472
Gussian low-pass Filter	37.254	38.703	36.112	37.405
Averaige Filter	37.212	38.605	36.034	30.019
Gussian noise	30.788	30.998	30.610	30.019
Salt and pepper noise	32.331	32.856	32.574	32.019
Speckle noise	36.558	36.476	34.9007	35.262
Cropping attack	10.666	6.0366	5.3850	10.566
JPG Compression	36.841	39.223	36.712	36.876
JPG2000 Compression	37.512	41.296	37.894	37.523
Rotation atatck	13.005	8.3514	7.2901	14.364
Motion Blur	31.571	30.726	29.122	33.232
HE	6.2522	11.058	11.217	10.702
Sharpening attack	35.174	37.452	35.145	36.059

Invisibility of attacked watermarked segment of 3-0-076 percent Noise and INU with watermark size 64X64

TABLE 5.8: Invisibility with size 64X64

Attacks	**CSF**	**GM**	**WM**	**RGB**
Median Filter	43.598	42.642	41.333	44.910
Gussian low-pass Filter	41.438	39.997	38.487	43.106
Averaige Filter	41.301	39.853	38.339	43.004
Gussian noise	32.058	31.302	31.403	30.773
Salt and pepper noise	32.385	33.588	33.811	34.089
Speckle noise	42.479	37.650	36.890	38.840
Cropping attack	11.126	6.0299	5.4250	10.687
JPG Compression	43.355	41.981	40.964	43.048
JPG2000 Compression	48.632	48.553	45.839	48.323
Rotation atatck	13.222	8.3683	7.3728	14.525
Motion Blur	30.882	30.882	29.414	34.349
HE	3.7953	10.882	9.1836	10.335
Sharpening attack	40.778	40.210	38.814	42.595

Invisibility of attacked watermarked segment of 3-0-076 percent Noise and INU with watermark size 128X128

TABLE 5.9: Invisibility with size 128X128

Attacks	**CSF**	**GM**	**WM**	**RGB**
Median Filter	13.808	6.0904	6.6064	9.4171
Gussian low-pass Filter	13.956	6.1459	6.6875	9.4711
Averaige Filter	13.956	6.1458	6.6874	9.4711
Gussian noise	14.022	6.2501	6.7775	9.6568
Salt and pepper noise	13.889	6.1380	6.6757	9.4605
Speckle noise	13.937	6.1409	6.6799	9.4684
Cropping attack	13.666	6.1322	6.6193	9.4468
JPG Compression	13.979	6.1544	6.6995	9.4698
JPG2000 Compression	13.951	6.1509	6.6940	9.4785
Rotation atatck	13.696	6.1169	6.6205	9.4131
Motion Blur	13.940	6.1425	6.6823	9.4672
HE	1.8900	4.8668	5.0186	4.8637
Sharpening attack	14.023	6.1745	6.7316	9.5050

Invisibility of attacked watermarked segment of 3-0-076 percent Noise and INU with watermark size 256X256

TABLE 5.10: Invisibility with size 256X256

Attacks	**CSF**	**GM**	**WM**	**RGB**
Median Filter	37.461	39.569	38.918	37.462
Gussian low-pass Filter	37.256	38.692	36.096	37.398
Averaige Filter	37.219	38.594	36.019	37.377
Gussian noise	30.769	31.001	30.632	30.002
Salt and pepper noise	31.004	32.846	32.002	32.201
Speckle noise	36.531	36.400	34.874	35.284
Cropping attack	10.921	6.0155	5.3657	10.530
JPG Compression	36.848	39.174	36.657	36.867
JPG2000 Compression	37.493	41.215	37.809	37.521
Rotation atatck	12.087	8.3704	7.3292	14.400
Motion Blur	31.576	30.741	29.127	33.214
HE	6.2642	11.069	11.263	10.691
Sharpening attack	35.134	37.439	35.120	36.044

Invisibility of attacked watermarked segment of 5-0-076 percent Noise and INU with watermark size 64X64

TABLE 5.11: Invisibility with size 64X64

Attacks	**CSF**	**GM**	**WM**	**RGB**
Median Filter	43.515	42.375	41.059	44.873
Gussian low-pass Filter	41.381	39.826	38.314	43.067
Averaige Filter	41.246	39.680	38.168	42.962
Gussian noise	31.997	31.312	31.389	30.769
Salt and pepper noise	33.040	33.563	33.436	33.983
Speckle noise	42.498	37.692	36.847	38.860
Cropping attack	11.163	6.0460	5.4550	10.689
JPG Compression	43.384	41.915	40.851	43.002
JPG2000 Compression	48.598	48.362	45.757	48.260
Rotation atatck	13.213	8.3880	7.3850	14.501
Motion Blur	32.104	30.617	29.156	34.285
HE	3.6409	10.934	9.1734	10.319
Sharpening attack	40.757	40.041	38.637	42.560

Invisibility of attacked watermarked segment of 5-0-076 percent Noise and INU with watermark size 128X128

TABLE 5.12: Invisibility with size 128X128

Attacks	**CSF**	**GM**	**WM**	**RGB**
Median Filter	13.867	6.0702	6.6553	9.4347
Gussian low-pass Filter	14.019	6.1272	6.7386	9.4896
Averaige Filter	14.019	6.1272	6.7385	9.4896
Gussian noise	14.087	6.2310	6.8256	9.6777
Salt and pepper noise	13.951	6.1196	6.7264	9.4770
Speckle noise	13.999	6.1221	6.7308	9.4868
Cropping attack	13.723	6.1117	6.6663	9.4632
JPG Compression	14.042	6.1359	6.7488	9.4879
JPG2000 Compression	14.014	6.1319	6.7455	9.4964
Rotation atatck	13.751	6.0980	6.6680	9.4306
Motion Blur	14.002	6.1239	6.7332	9.4858
HE	1.8884	4.8791	5.0209	5.0236
Sharpening attack	14.087	6.1567	6.7839	9.5241

Invisibility of attacked watermarked segment of 5-0-076 percent Noise and INU with watermark size 256X256

TABLE 5.13: Invisibility with size 256X256

Attacks	**CSF**	**GM**	**WM**	**RGB**
Median Filter	37.465	39.405	36.754	37.459
Gussian low-pass Filter	37.253	38.558	35.940	37.388
Averaige Filter	37.216	38.456	35.861	37.366
Gussian noise	30.802	31.008	30.591	30.013
Salt and pepper noise	31.376	32.655	31.925	32.588
Speckle noise	36.576	36.468	34.789	35.256
Cropping attack	10.168	6.0321	5.3941	10.531
JPG Compression	36.828	39.161	36.546	36.860
JPG2000 Compression	37.493	41.190	37.693	37.496
Rotation atatck	12.077	8.3906	7.3395	14.376
Motion Blur	31.587	30.479	28.877	33.163
HE	6.1052	11.111	11.138	10.496
Sharpening attack	35.119	37.339	34.985	36.029

5.3.2 Structural Similarity Index Measure

Tables below depicts SSIM values to check the invisibility watermarked segmented candidate images of MRI with 0,1,3 and 5 percent Noise and INU level that were attacked. Invisibility of 64x64 watermark with SSIM of 0-0-076 percent Noise and INU.

Table 5.14: Invisibility with size 64x64

Attacks	**CSF**	**GM**	**WM**	**RGB**
Median Filter	0.9654	0.8104	0.9596	0.9820
Gussian low-pass Filter	0.9987	0.6245	0.7509	0.8764
Averaige Filter	0.8245	0.5229	0.7483	0.8747
Gussian noise	0.8192	0.0954	0.7229	0.7633
Salt and pepper noise	0.9913	0.8327	0.9829	0.9910
Speckle noise	0.9966	0.0654	0.9162	0.9957
Cropping attack	0.9557	0.9396	0.9174	0.9485
JPG Compression	0.9937	0.7300	0.9796	0.9947
JPG2000 Compression	0.9983	0.8408	0.9902	0.9974
Rotation atatck	0.2309	0.5819	0.4952	0.3626
Motion Blur	0.6029	0.4843	0.5965	0.7070
HE	0.8956	0.8429	0.8375	0.8956
Sharpening attack	0.9681	0.7401	0.9325	0.9664

Invisibility of 128x128 watermark with SSIM of 0-0-076 percent Noise and INU

Table 5.15: Invisibility with size 128X128

Attacks	**CSF**	**GM**	**WM**	**RGB**
Median Filter	0.3073	0.3658	0.3723	0.3418
Gussian low-pass Filter	0.7153	0.6806	0.7025	0.6901
Averaige Filter	0.7151	0.6799	0.7018	0.6885
Gussian noise	0.8777	0.8516	0.8430	0.9068
Salt and pepper noise	0.8227	0.7780	0.7738	0.8531
Speckle noise	0.7998	0.7519	0.7542	0.7946
Cropping attack	0.9005	0.8551	0.8687	0.8858
JPG Compression	0.8835	0.8146	0.8191	0.8339
JPG2000 Compression	0.8183	0.7739	0.7788	0.8117
Rotation atatck	0.1314	0.4742	0.5559	0.1507
Motion Blur	0.7201	0.6978	0.7112	0.7140
HE	0.8903	0.8903	0.8903	0.8903
Sharpening attack	0.9757	0.9667	0.9571	0.9564

Invisibility of 1256x256 watermark with SSIM of 0-0-076 percent Noise and INU

Table 5.16: Invisibility with size 256X256

Attacks	**CSF**	**GM**	**WM**	**RGB**
Median Filter	0.9817	0.8202	0.9620	0.9923
Gussian low-pass Filter	0.9189	0.6016	0.8353	0.9591
Averaige Filter	0.9163	0.5976	0.8325	0.9581
Gussian noise	0.9127	0.4683	0.8359	0.8992
Salt and pepper noise	0.9451	0.7312	0.9379	0.9607
Speckle noise	0.9926	0.4163	0.9479	0.9839
Cropping attack	0.9226	0.8913	0.8715	0.9098
JPG Compression	0.9953	0.8372	0.9851	0.9939
JPG2000 Compression	0.9981	0.8867	0.9933	0.9998
Rotation atatck	0.3115	0.5621	0.5525	0.5956
Motion Blur	0.7297	0.4662	0.6830	0.8214
HE	0.8853	0.8137	0.8083	0.8853
Sharpening attack	0.9821	0.8262	0.9618	0.9860

Invisibility of 64x64 watermark with SSIM of 1-0-076 percent Noise and INU

Table 5.17: Invisibility with size 64X64

Attacks	**CSF**	**GM**	**WM**	**RGB**
Median Filter	0.9678	0.7999	0.9495	0.9707
Gussian low-pass Filter	0.8398	0.5245	0.7499	0.8756
Averaige Filter	0.8360	0.5227	0.7474	0.8737
Gussian noise	0.8342	0.0958	0.7279	0.7662
Salt and pepper noise	0.9946	0.8017	0.9867	0.9914
Speckle noise	0.9974	0.0647	0.9017	0.9957
Cropping attack	0.9574	0.9389	0.9250	0.9478
JPG Compression	0.9916	0.7251	0.9756	0.9950
JPG2000 Compression	0.9987	0.8406	0.9903	0.9969
Rotation atatck	0.2357	0.5815	0.5049	0.3658
Motion Blur	0.6131	0.4849	0.5956	0.7071
HE	0.8956	0.8432	0.8372	0.8956
Sharpening attack	0.9707	0.7389	0.9321	0.9678

Invisibility of 128x128 watermark with SSIM of 1-0-076 percent Noise and INU

Table 5.18: Invisibility with size 128X128

Attacks	**CSF**	**GM**	**WM**	**RGB**
Median Filter	0.3064	0.3654	0.3726	0.3424
Gussian low-pass Filter	0.7150	0.6811	0.7032	0.6914
Averaige Filter	0.7142	0.6804	0.7024	0.6900
Gussian noise	0.8833	0.8529	0.8441	0.9049
Salt and pepper noise	0.8318	0.7788	0.7758	0.8354
Speckle noise	0.8003	0.7542	0.7553	0.7951
Cropping attack	0.8986	0.8565	0.8665	0.8854
JPG Compression	0.8828	0.8172	0.8198	0.8357
JPG2000 Compression	0.8204	0.7732	0.7797	0.8131
Rotation atatck	0.1273	0.4746	0.5564	0.1532
Motion Blur	0.7191	0.6984	0.7117	0.7148
HE	0.8903	0.8903	0.8903	0.8903
Sharpening attack	0.9760	0.9671	0.9575	0.9569

Invisibility of 256x256 watermark with SSIM of 1-0-076 percent Noise and INU

Table 5.19: Invisibility with size 256X256

Attacks	**CSF**	**GM**	**WM**	**RGB**
Median Filter	0.9848	0.8190	0.9625	0.9923
Gussian low-pass Filter	0.9269	0.5990	0.8356	0.9590
Averaige Filter	0.9246	0.5950	0.8328	0.9580
Gussian noise	0.9273	0.4671	0.8368	0.9005
Salt and pepper noise	0.9552	0.7312	0.9395	0.9600
Speckle noise	0.9959	0.4193	0.9485	0.9839
Cropping attack	0.9222	0.8906	0.8750	0.9096
JPG Compression	0.9969	0.8353	0.9851	0.9936
JPG2000 Compression	0.9999	0.8850	0.9935	0.9997
Rotation atatck	0.3147	0.5612	0.5584	0.5992
Motion Blur	0.7460	0.4652	0.6837	0.8215
HE	0.8853	0.8138	0.8082	0.8853
Sharpening attack	0.9843	0.8248	0.9620	0.9858

Invisibility of 64x64 watermark with SSIM of 3-0-076 percent Noise and INU

TABLE 5.20: Invisibility with size 64X64

Attacks	**CSF**	**GM**	**WM**	**RGB**
Median Filter	0.9738	0.8040	0.9496	0.9713
Gussian low-pass Filter	0.8441	0.5265	0.7530	0.8767
Averaige Filter	0.8402	0.5242	0.7504	0.9749
Gussian noise	0.8358	0.0910	0.7280	0.7578
Salt and pepper noise	0.9944	0.8313	0.9872	0.9908
Speckle noise	0.9976	0.0657	0.9095	0.9952
Cropping attack	0.9653	0.9387	0.9292	0.9494
JPG Compression	0.9927	0.7124	0.9794	0.9952
JPG2000 Compression	0.9979	0.8391	0.9907	0.9973
Rotation atatck	0.2312	0.5832	0.5217	0.3584
Motion Blur	0.6203	0.4847	0.5979	0.7119
HE	0.8956	0.8423	0.8376	0.8956
Sharpening attack	0.9717	0.7442	0.9343	0.9684

Invisibility of 128x128 watermark with SSIM of 3-0-076 percent Noise and INU

TABLE 5.21: Invisibility with size 128X128

Attacks	**CSF**	**GM**	**WM**	**RGB**
Median Filter	0.3018	0.3665	0.3750	0.3417
Gussian low-pass Filter	0.7155	0.6809	0.7039	0.6902
Averaige Filter	0.7148	0.6803	0.7034	0.6890
Gussian noise	0.8780	0.8511	0.8442	0.9054
Salt and pepper noise	0.8262	0.7798	0.7737	0.8464
Speckle noise	0.7998	0.7510	0.7555	0.7943
Cropping attack	0.9075	0.8579	0.8708	0.8920
JPG Compression	0.8818	0.8156	0.8204	0.8350
JPG2000 Compression	0.8200	0.7724	0.7780	0.8105
Rotation atatck	0.1297	0.4774	0.5567	0.1544
Motion Blur	0.7205	0.6975	0.7128	0.7144
HE	0.8903	0.8903	0.8903	0.8903
Sharpening attack	0.9761	0.9657	0.9569	0.9568

Invisibility of 256x256 watermark with SSIM of 3-0-076 percent Noise and INU

Table 5.22: Invisibility with size 256X256

Attacks	**CSF**	**GM**	**WM**	**RGB**
Median Filter	0.9858	0.8199	0.9621	0.9924
Gussian low-pass Filter	0.9277	0.6030	0.8364	0.9593
Averaige Filter	0.9254	0.5989	0.8337	0.9583
Gussian noise	0.9251	0.4698	0.8415	0.8998
Salt and pepper noise	0.9497	0.7487	0.9408	0.9605
Speckle noise	0.9961	0.4267	0.9498	0.9840
Cropping attack	0.9247	0.8917	0.876	0.9110
JPG Compression	0.9927	0.8367	0.9853	0.9939
JPG2000 Compression	0.9979	0.8879	0.9939	0.9998
Rotation atatck	0.2312	0.5661	0.5677	0.6074
Motion Blur	0.6203	0.4684	0.6862	0.8211
HE	0.8956	0.8137	0.8085	0.8854
Sharpening attack	0.9717	0.8261	0.9624	0.9861

Invisibility of 64x64 watermark with SSIM of 5-0-076 percent Noise and INU

Table 5.23: Invisibility with size 64X64

Attacks	**CSF**	**GM**	**WM**	**RGB**
Median Filter	0.9703	0.8021	0.9492	0.9705
Gussian low-pass Filter	0.8420	0.5279	0.7569	0.8766
Averaige Filter	0.8383	0.5265	0.7544	0.8746
Gussian noise	0.8336	0.0996	0.7488	0.7722
Salt and pepper noise	0.9920	0.8281	0.9854	0.9921
Speckle noise	0.9970	0.0663	0.9426	0.9963
Cropping attack	0.9639	0.9405	0.9318	0.9498
JPG Compression	0.9921	0.6997	0.9804	0.9943
JPG2000 Compression	0.9981	0.8302	0.9902	0.9974
Rotation atatck	0.2178	0.5847	0.5847	0.3577
Motion Blur	0.6180	0.4869	0.6034	0.7120
HE	0.8956	0.8409	0.8393	0.8956
Sharpening attack	0.9708	0.7380	0.9326	0.9685

Invisibility of 128x128 watermark with SSIM of 5-0-076 percent Noise and INU

TABLE 5.24: Invisibility with size 128X128

Attack	**CSF**	**GM**	**WM**	**RGB**
Median Filter	0.3001	0.3649	0.3770	0.3414
Gussian low-pass Filter	0.7069	0.6848	0.7119	0.6926
Averaige Filter	0.7063	0.6843	0.7110	0.6913
Gussian noise	0.8773	0.8537	0.8474	0.9051
Salt and pepper noise	0.8233	0.7811	0.7828	0.8336
Speckle noise	0.7975	0.7562	0.7637	0.7965
Cropping attack	0.8911	0.8686	0.8742	0.8853
JPG Compression	0.8776	0.8216	0.8220	0.8390
JPG2000 Compression	0.8177	0.7757	0.7869	0.8132
Rotation atatck	0.1235	0.4900	0.5740	0.1611
Motion Blur	0.7134	0.6999	0.7203	0.7169
HE	0.8903	0.8903	0.8903	0.8903
Sharpening attack	0.9759	0.9679	0.9582	0.9580

Invisibility of 256x256 watermark with SSIM of 5-0-076 percent Noise and INU

TABLE 5.25: Invisibility with size 256X256

Attack	**CSF**	**GM**	**WM**	**RGB**
Median Filter	0.9848	0.8142	0.9605	0.9919
Gussian low-pass Filter	0.9269	0.6002	0.8387	0.9584
Averaige Filter	0.9246	0.5962	0.8359	0.9547
Gussian noise	0.9271	0.4727	0.8510	0.9016
Salt and pepper noise	0.9634	0.7530	0.9407	0.9517
Speckle noise	0.9961	0.4240	0.9550	0.9837
Cropping attack	0.9244	0.8924	0.8786	0.9106
JPG Compression	0.9967	0.8343	0.9865	0.9937
JPG2000 Compression	0.9999	0.8857	0.9944	0.9998
Rotation atatck	0.2978	0.5658	0.5720	0.6065
Motion Blur	0.7473	0.4699	0.6894	0.8203
HE	0.8853	0.8123	0.8107	0.8854
Sharpening attack	0.9847	0.8244	0.9625	0.9858

5.4 Robustness of Attacked Watermarked Image

After the invisibility has been determined to be acceptable, the robustness must be evaluated further. Robustness refers to a system's ability to withstand change without changing its initial, stable configuration.

Robustness in image watermark-ing refers to the ability to extract watermarks from watermarked host images under a variety of attacks.As a result, it's critical to test the robustness of an image watermarking technol-ogy.

The quality of the recovered watermarks is tested when the watermarked images are subjected to various attacks in order to assess the resilience of the suggested approach.

Proposed approach is also robust against many attacks, results are shown below.Robustness of 64x64 extracted watermark from attacked watermarked segments of 0-0-076 percent Noise and INU

TABLE 5.26: Robustness with size 64X64

Attacks	**CSF**	**GM**	**WM**	**RGB**
Median Filter	0.9654	0.8004	0.9496	0.9720
Gussian low-pass Filter	0.9987	0.5245	0.7509	0.8764
Averaige Filter	0.8245	0.5229	0.7483	0.8747
Gussian noise	0.8192	0.0954	0.7229	0.7633
Salt and pepper noise	0.9923	0.8327	0.9829	0.9910
Speckle noise	0.9966	0.0654	0.9162	0.9957
Cropping attack	0.9557	0.9396	0.9174	0.9485
JPG Compression	0.9937	0.7300	0.9796	0.9947
JPG2000 Compression	0.9983	0.8408	0.9902	0.9974
Rotation atatck	0.2309	0.5819	0.4952	0.3626
Motion Blur	0.6029	0.4843	0.5965	0.7070
HE	0.8956	0.8429	0.8375	0.8956
Sharpening attack	0.9681	0.7401	0.9325	0.9664

Robustness of 128X128 extracted watermark from attacked watermarked segments of 0-0-076 percent noise and inu

TABLE 5.27: Robustness with size 128X128

Attacks	**CSF**	**GM**	**WM**	**RGB**
Median Filter	0.3073	0.3658	0.3723	0.3418
Gussian low-pass Filter	0.7153	0.6806	0.7025	0.6901
Averaige Filter	0.7151	0.6799	0.7018	0.6885
Gussian noise	0.8777	0.8516	0.8430	0.9068
Salt and pepper noise	0.8227	0.7780	0.7738	0.8531
Speckle noise	0.7998	0.7519	0.7542	0.7946
Cropping attack	0.9005	0.8551	0.8687	0.8858
JPG Compression	0.8835	0.8146	0.8191	0.8339
JPG2000 Compression	0.8183	0.7739	0.7788	0.8117
Rotation atatck	0.1314	0.4742	0.5559	0.1507
Motion Blur	0.7201	0.6978	0.7112	0.7140
HE	0.8903	0.8903	0.8903	0.8903
Sharpening attack	0.9757	0.9667	0.9571	0.9564

Robustness of 256X256 extracted watermark from attacked watermarked segments of 0-0-076 percent noise and inu

TABLE 5.28: Robustness with size 256X256

Attacks	**CSF**	**GM**	**WM**	**RGB**
Median Filter	0.9817	0.8202	0.9620	0.9923
Gussian low-pass Filter	0.9189	0.6016	0.8353	0.9591
Averaige Filter	0.9163	0.5976	0.8325	0.9581
Gussian noise	0.9127	0.4683	0.8359	0.8992
Salt and pepper noise	0.9451	0.7312	0.9379	0.9607
Speckle noise	0.9926	0.4163	0.9479	0.9839
Cropping attack	0.9226	0.8913	0.8715	0.9098
JPG Compression	0.9953	0.8372	0.9851	0.9939
JPG2000 Compression	0.9981	0.8867	0.9933	0.9998
Rotation atatck	0.3115	0.5621	0.5525	0.5956
Motion Blur	0.7297	0.4662	0.6830	0.8214
HE	0.8853	0.8137	0.8083	0.8853
Sharpening attack	0.9821	0.8262	0.9618	0.9860

Robustness of 64X64 extracted watermark from attacked watermarked segments of 1-0-076 percent noise and inu

TABLE 5.29: Robustness with size 64X64

Attacks	**CSF**	**GM**	**WM**	**RGB**
Median Filter	0.9678	0.7999	0.9495	0.9707
Gussian low-pass Filter	0.8398	0.5245	0.7499	0.8756
Averaige Filter	0.8360	0.5227	0.7474	0.8737
Gussian noise	0.8342	0.0958	0.7279	0.7662
Salt and pepper noise	0.9946	0.8017	0.9867	0.9914
Speckle noise	0.9974	0.0647	0.9017	0.9957
Cropping attack	0.9574	0.9389	0.9250	0.9478
JPG Compression	0.9916	0.7251	0.9756	0.9950
JPG2000 Compression	0.9987	0.8406	0.9903	0.9969
Rotation atatck	0.2357	0.5815	0.5049	0.3658
Motion Blur	0.6131	0.4849	0.5956	0.7071
HE	0.8956	0.8432	0.8372	0.8956
Sharpening attack	0.9707	0.7389	0.9321	0.9678

Robustness of 128X128 extracted watermark from attacked watermarked segments of 1-0-076 percent noise and inu

TABLE 5.30: Robustness with size 128X128

Attacks	**CSF**	**GM**	**WM**	**RGB**
Median Filter	0.3064	0.3654	0.3726	0.3424
Gussian low-pass Filter	0.7150	0.6811	0.7032	0.6914
Averaige Filter	0.7142	0.6804	0.7024	0.6900
Gussian noise	0.8833	0.8529	0.8441	0.9049
Salt and pepper noise	0.8318	0.7788	0.7758	0.8354
Speckle noise	0.8003	0.7542	0.7553	0.7951
Cropping attack	0.8986	0.8565	0.8665	0.8854
JPG Compression	0.8828	0.8172	0.8198	0.8357
JPG2000 Compression	0.8204	0.7732	0.7797	0.8131
Rotation atatck	0.1273	0.4746	0.5564	0.1532
Motion Blur	0.7191	0.6984	0.7117	0.7148
HE	0.8903	0.8903	0.8903	0.8903
Sharpening attack	0.9760	0.9671	0.9575	0.9569

Robustness of 256X256 extracted watermark from attacked watermarked segments of 1-0-076 percent noise and inu

TABLE 5.31: Robustness with size 256X256

Attacks	**CSF**	**GM**	**WM**	**RGB**
Median Filter	0.9848	0.8190	0.9625	0.9923
Gussian low-pass Filter	0.9269	0.5990	0.8356	0.9590
Averaige Filter	0.9246	0.5950	0.8328	0.9580
Gussian noise	0.9273	0.4671	0.8368	0.9005
Salt and pepper noise	0.9552	0.7312	0.9395	0.9600
Speckle noise	0.9959	0.4193	0.9485	0.9839
Cropping attack	0.9222	0.8906	0.8750	0.9096
JPG Compression	0.9969	0.8353	0.9851	0.9936
JPG2000 Compression	0.9999	0.8850	0.9935	0.9997
Rotation atatck	0.3147	0.5612	0.5584	0.5992
Motion Blur	0.7460	0.4652	0.6837	0.8215
HE	0.8853	0.8138	0.8082	0.8853
Sharpening attack	0.9843	0.8248	0.9620	0.9858

Robustness of 64X64 extracted watermark from attacked watermarked segments of 3-0-076 percent noise and inu

TABLE 5.32: Robustness with size 64X64

Attacks	**CSF**	**GM**	**WM**	**RGB**
Median Filter	0.9738	0.8040	0.9496	0.9713
Gussian low-pass Filter	0.8441	0.5265	0.7530	0.8767
Averaige Filter	0.8402	0.5242	0.7504	0.9749
Gussian noise	0.8358	0.0910	0.7280	0.7578
Salt and pepper noise	0.9944	0.8313	0.9872	0.9908
Speckle noise	0.9976	0.0657	0.9095	0.9952
Cropping attack	0.9653	0.9387	0.9292	0.9494
JPG Compression	0.9927	0.7124	0.9794	0.9952
JPG2000 Compression	0.9979	0.8391	0.9907	0.9973
Rotation atatck	0.2312	0.5832	0.5217	0.3584
Motion Blur	0.6203	0.4847	0.5979	0.7119
HE	0.8956	0.8423	0.8376	0.8956
Sharpening attack	0.9717	0.7442	0.9343	0.9684

Robustness of 128X128 extracted watermark from attacked watermarked segments of 3-0-076 percent noise and inu

Table 5.33: Robustness with size 128X128

Attacks	**CSF**	**GM**	**WM**	**RGB**
Median Filter	0.3018	0.3665	0.3750	0.3417
Gussian low-pass Filter	0.7155	0.6809	0.7039	0.6902
Averaige Filter	0.7148	0.6803	0.7034	0.6890
Gussian noise	0.8780	0.8511	0.8442	0.9054
Salt and pepper noise	0.8262	0.7798	0.7737	0.8464
Speckle noise	0.7998	0.7510	0.7555	0.7943
Cropping attack	0.9075	0.8579	0.8708	0.8920
JPG Compression	0.8818	0.8156	0.8204	0.8350
JPG2000 Compression	0.8200	0.7724	0.7780	0.8105
Rotation atatck	0.1297	0.4774	0.5567	0.1544
Motion Blur	0.7205	0.6975	0.7128	0.7144
HE	0.8903	0.8903	0.8903	0.8903
Sharpening attack	0.9761	0.9657	0.9569	0.9568

Robustness of 256X256 extracted watermark from attacked watermarked segments of 3-0-076 percent noise and inu

Table 5.34: Robustness with size 256X256

Attacks	**CSF**	**GM**	**WM**	**RGB**
Median Filter	0.9858	0.8199	0.9621	0.9924
Gussian low-pass Filter	0.9277	0.6030	0.8364	0.9593
Averaige Filter	0.9254	0.5989	0.8337	0.9583
Gussian noise	0.9251	0.4698	0.8415	0.8998
Salt and pepper noise	0.9497	0.7487	0.9408	0.9605
Speckle noise	0.9961	0.4267	0.9498	0.9840
Cropping attack	0.9247	0.8917	0.876	0.9110
JPG Compression	0.9927	0.8367	0.9853	0.9939
JPG2000 Compression	0.9979	0.8879	0.9939	0.9998
Rotation atatck	0.2312	0.5661	0.5677	0.6074
Motion Blur	0.6203	0.4684	0.6862	0.8211
HE	0.8956	0.8137	0.8085	0.8854
Sharpening attack	0.9717	0.8261	0.9624	0.9861

Robustness of 64X64 extracted watermark from attacked watermarked segments of 5-0-076 percent noise and inu

TABLE 5.35: Robustness with size 64X64

Attacks	**CSF**	**GM**	**WM**	**RGB**
Median Filter	0.9703	0.8021	0.9492	0.9705
Gussian low-pass Filter	0.8420	0.5279	0.7569	0.8766
Averaige Filter	0.8383	0.5265	0.7544	0.8746
Gussian noise	0.8336	0.0996	0.7488	0.7722
Salt and pepper noise	0.9920	0.8281	0.9854	0.9921
Speckle noise	0.9970	0.0663	0.9426	0.9963
Cropping attack	0.9639	0.9405	0.9318	0.9498
JPG Compression	0.9921	0.6997	0.9804	0.9943
JPG2000 Compression	0.9981	0.8302	0.9902	0.9974
Rotation atatck	0.2178	0.5847	0.5847	0.3577
Motion Blur	0.6180	0.4869	0.6034	0.7120
HE	0.8956	0.8409	0.8393	0.8956
Sharpening attack	0.9708	0.7380	0.9326	0.9685

Robustness of 128X128 extracted watermark from attacked watermarked segments of 5-0-076 percent noise and inu

TABLE 5.36: Robustness with size 128X128

Attack	**CSF**	**GM**	**WM**	**RGB**
Median Filter	0.3001	0.3649	0.3770	0.3414
Gussian low-pass Filter	0.7069	0.6848	0.7119	0.6926
Averaige Filter	0.7063	0.6843	0.7110	0.6913
Gussian noise	0.8773	0.8537	0.8474	0.9051
Salt and pepper noise	0.8233	0.7811	0.7828	0.8336
Speckle noise	0.7975	0.7562	0.7637	0.7965
Cropping attack	0.8911	0.8686	0.8742	0.8853
JPG Compression	0.8776	0.8216	0.8220	0.8390
JPG2000 Compression	0.8177	0.7757	0.7869	0.8132
Rotation atatck	0.1235	0.4900	0.5740	0.1611
Motion Blur	0.7134	0.6999	0.7203	0.7169
HE	0.8903	0.8903	0.8903	0.8903
Sharpening attack	0.9759	0.9679	0.9582	0.9580

Robustness of 256X256 extracted watermark from attacked watermarked segments of 5-0-076 percent noise and inu

TABLE 5.37: Robustness with size 256X256

Attack	**CSF**	**GM**	**WM**	**RGB**
Median Filter	0.9848	0.8142	0.9605	0.9919
Gussian low-pass Filter	0.9269	0.6002	0.8387	0.9584
Averaige Filter	0.9246	0.5962	0.8359	0.9547
Gussian noise	0.9271	0.4727	0.8510	0.9016
Salt and pepper noise	0.9634	0.7530	0.9407	0.9517
Speckle noise	0.9961	0.4240	0.9550	0.9837
Cropping attack	0.9244	0.8924	0.8786	0.9106
JPG Compression	0.9967	0.8343	0.9865	0.9937
JPG2000 Compression	0.9999	0.8857	0.9944	0.9998
Rotation atatck	0.2978	0.5658	0.5720	0.6065
Motion Blur	0.7473	0.4699	0.6894	0.8203
HE	0.8853	0.8123	0.8107	0.8854
Sharpening attack	0.9847	0.8244	0.9625	0.9858

5.5 Discussions

This section is to discuss results presented above

Results presented above shows that during segmentation images with low noise level and INU produce better result as compared to the images with high noise and INU level ,this noise level also has little effect on watermarking process .Tbles above also depicts invisibility of the watermarked segmented host images of MRI with 0,1,3 and 5 percent Noise and INU level that were not attacked, as well as the extracted watermarks with watermark sizes of 256 x 256, 128 x 128, and 64 x 64. result shows that invisibility of segmented host images in case of no attack with incresing noise and inu is better for 256x256 and 64x64 size except with size 128x128 in case of size 128x128 results are meeting criteria of invisibility .Results also describes that segmented part GM has better results than CSF,WM and RGB except with size 128x128 . Invisibility of Attacked Watermarked Image of

different size 64x64, 128x128 and 256x256 under verious attacks spoof attacks, such as the filter, n oise, J PEG c ompression,JPEG2000 c ompression, a nd sharpening attacks also shown in results ,in case of image with 128x128 size got poor results and got better acceptable result for some attacks with RGB segments with all noise level. The quality of the recovered watermarks is tested when the watermarked images are subjected to various attacks in order to assess the resilience of the suggested approach. Proposed approach is also robust against many attacks in case CSF 256x256 and 64x64 more robust than GM and WM , as shown above.

Chapter 6

Conclusion and Future Work

6.1 Introduction

Medical images hold confidential property and are very crucial and important part of medical information. Electronic transmission of the medical images is one of the primary requirements in a typical Electronic-Healthcare (E-Healthcare) system.However, this transmission could be liable to hackers who may modify the whole medical image or only a part of it during transit.

To guarantee the integrity of a medical image, digital watermarking is important technique.There is need to know which information should be watermarked so important information from medical image should be extracted through segmentation.Technique proposed in this study include two main steps segmentation and watermarking.The water-marked host image should be invisible to humans to ensure the safety of infor-mation, hence the watermark invisibility is an important metric to measure the performance.The robustness needs to be further evaluated when the invisibility is acceptable.Detailed literature review shows that lot of work carried out domain of medical image watermarking but there is still need to consider images that carry certain level of complexities ,also there is need to improve level of robustness and imperceptibility .This research focused on solution to watermark Brain MRI with

different Noise and INU level and maintain its robustness and Invisibility under different attacks in all cases.

The research work can be concluded as:

1 The most of techniques found in literature used for segmentation of images and each technique works efficiently in different cases to segment images. ANN is trained in default setting to perform segmentation in this study as according to the best of our knowledge ANN has became one of the most widely acknowledged tool for processing medical images and according to the search results with Google Scholar, more than 33,000 items were found on the topic of medical image processing by using ANNs.

2 literature review shows there are lots of techniques for watermarking but still there is need of improvement to make medical images more secure by improving level of robustness and imperceptibility.

3 The proposed technique is combination of trained ANN in default setting for segmenting images and dwt-svd-hd for embedding and extracting watermark after performing various attacks. The numerical simulation experiments examine the method's invisibility and robustness.

4 It can be concluded that watermarked host image exhibit good visual quality, PSNRs, and SSIMs, for images with all noise level under different attacks except for rotation attack and cropping attack , histogram equalizing attacks.

5 Furthermore, with reasonably high NCs, the watermarks can be clearly retrieved from the watermarked host image under various attacks. Proposed approach is also robust against many attacks except rotation attack and cropping attack , histogram equalizing attacks.

6 Furthermore, the suggested image watermarking approach may achieve good invisibility and robustness even for watermarks of various sizes except for watermark 128x128 .

Following are some of the potential directions for future research in this area that are identified:

1 Technique used in this study work well for images of all noise level but does not work well for watermark image with size 128x128 in case of invisibility and robustness. Improve this technique to get better results for watermark size 128x128 also.

2 This technique is resisting some of attacks for all noise level segmented (CSF, GM and WM) images but not all attacks. Improve this technique so that it can resist more attacks like rotation, motion blur, cropping and histogram equalization etc.

Bibliography

[1] M. Begum, "Analysis of digital image watermarking techniques through hybrid methods," *Advances in Multimedia*, vol. 4, pp. 420–433, 2020.

[2] A. R. N. Nilchi and A. Taheri, "A new robust digital image watermarking technique based on the discrete cosine transform and neural network," *International Symposium on Biometrics and Security Technologies*, vol. 81, pp. 563–571, 2008.

[3] V. M. D. S. . M. G. S. Nikolaos V. Boulgouris, Ioannis Kompatsiaris, "Segmentation and content-based watermarking for color image and image region indexing and retrieval," *EURASIP J. Adv. Signal Process*, vol. 4, pp. 420–433, 2002.

[4] J.-S. Pao-TaYu, Hung-HsuTsai, "Digital watermarking based on neural networks for color images," *Signal Processing*, vol. 81, pp. 663–671, 2001.

[5] I. Despotović, B. Goossens, and W. Philips, "Mri segmentation of the human brain: challenges, methods, and applications," *Computational and mathematical methods in medicine*, vol. 2015, pp. 440–455, 2015.

[6] A. Mahbod, M. Chowdhury, Ö. Smedby, and C. Wang, "Automatic brain segmentation using artificial neural networks with shape context," *Pattern Recognition Letters*, vol. 101, pp. 74–79, 2018.

[7] S. Yuheng and Y. Hao, "Image segmentation algorithms overview," *arXiv preprint arXiv:1707.02051*, vol. 10, pp. 70–79, 2017.

[8] C. Amza, "A review on neural network-based image segmentation techniques," *De Montfort University, Mechanical and Manufacturing Engg., The Gateway Leicester, LE1 9BH, United Kingdom*, vol. 11, pp. 1–23, 2012.

[9] I. Scholl, T. Aach, T. M. Deserno, and T. Kuhlen, "Challenges of medical image processing," *Computer science-Research and development*, vol. 26, no. 1, pp. 5–13, 2011.

[10] A. J. Worth and D. N. Kennedy, "Segmentation of magnetic resonance brain images using analogue constraint satisfaction neural networks," *Image and Vision Computing*, vol. 12, no. 6, pp. 345–354, 1994.

[11] D. Kaur and Y. Kaur, "Various image segmentation techniques: a review," *International Journal of Computer Science and Mobile Computing*, vol. 3, no. 5, pp. 809–814, 2014.

[12] A. Işın, C. Direkoğlu, and M. Şah, "Review of mri-based brain tumor image segmentation using deep learning methods," *Procedia Computer Science*, vol. 102, pp. 317–324, 2016.

[13] T. Zuva, O. O. Olugbara, S. O. Ojo, and S. M. Ngwira, "Image segmentation, available techniques, developments and open issues," *Canadian Journal on Image Processing and Computer Vision*, vol. 2, no. 3, pp. 20–29, 2011.

[14] D. J. Withey and Z. J. Koles, "Medical image segmentation: Methods and software," in *2007 Joint Meeting of the 6th International Symposium on Noninvasive Functional Source Imaging of the Brain and Heart and the International Conference on Functional Biomedical Imaging*, vol. 14, pp. 140–143, IEEE, 2007.

[15] M. N. Ahmed and A. A. Farag, "Two-stage neural network for volume segmentation of medical images," *Pattern Recognition Letters*, vol. 18, no. 11-13, pp. 1143–1151, 1997.

[16] W. E. Reddick, J. O. Glass, E. N. Cook, T. D. Elkin, and R. J. Deaton, "Automated segmentation and classification of multispectral magnetic resonance images of brain using artificial neural networks," *IEEE Transactions on medical imaging*, vol. 16, no. 6, pp. 911–918, 1997.

[17] J. Ning, L. Zhang, D. Zhang, and C. Wu, "Interactive image segmentation by maximal similarity based region merging," *Pattern Recognition*, vol. 43, no. 2, pp. 445–456, 2010.

[18] Z. Huang, X. Wang, J. Wang, W. Liu, and J. Wang, "Weakly-supervised semantic segmentation network with deep seeded region growing," in *Proceedings of the IEEE Conference on Computer Vision and Pattern Recognition*, vol. 45, pp. 7014–7023, 2018.

[19] D. Q. Zeebaree, H. Haron, A. M. Abdulazeez, and D. A. Zebari, "Machine learning and region growing for breast cancer segmentation," in *2019 International Conference on Advanced Science and Engineering (ICOASE)*, vol. 33, pp. 88–93, IEEE, 2019.

[20] W. Tao, H. Jin, and Y. Zhang, "Color image segmentation based on mean shift and normalized cuts," *IEEE Transactions on Systems, Man, and Cybernetics, Part B (Cybernetics)*, vol. 37, no. 5, pp. 1382–1389, 2007.

[21] W.-X. Kang, Q.-Q. Yang, and R.-P. Liang, "The comparative research on image segmentation algorithms," in *2009 First International Workshop on Education Technology and Computer Science*, vol. 2, pp. 703–707, IEEE, 2009.

[22] D. J. Bora and A. K. Gupta, "A novel approach towards clustering based image segmentation," *arXiv preprint arXiv:1506.01710*, vol. 4, pp. 101–110, 2015.

[23] R. B. Aghdam, A. S. B. Ghiasi, P. Fatemi, N. S. Hashemi, *et al.*, "Challenges in brain magnetic resonance image segmentation," *American Scientific Research Journal for Engineering, Technology, and Sciences (ASRJETS)*, vol. 27, no. 1, pp. 122–138, 2017.

[24] P. Jaiswal, N. K. Gupta, and A. Ambikapathy, "Comparative study of various training algorithms of artificial neural network," in *2018 International Conference on Advances in Computing, Communication Control and Networking (ICACCCN)*, vol. 25, pp. 1097–1101, IEEE, 2018.

[25] N. Coskun and T. Yildirim, "The effects of training algorithms in mlp network on image classification," in *Proceedings of the International Joint Conference on Neural Networks, 2003.*, vol. 2, pp. 1223–1226, IEEE, 2003.

[26] P. Chopra, R. K. Sharma, M. Kumar, *et al.*, "Artificial neural networks for the prediction of compressive strength of concrete," *International journal of applied science and engineering*, vol. 13, no. 3, pp. 187–204, 2015.

[27] E.-S. A. El-Dahshan, H. M. Mohsen, K. Revett, and A.-B. M. Salem, "Computer-aided diagnosis of human brain tumor through mri: A survey and a new algorithm," *Expert systems with Applications*, vol. 41, no. 11, pp. 5526–5545, 2014.

[28] B. Srinivas and G. S. Rao, "Performance evaluation of fuzzy c means segmentation and support vector machine classification for mri brain tumor," in *Soft computing for problem solving*, vol. 11, pp. 355–367, Springer, 2019.

[29] J. Song and Z. Zhang, "A modified robust fcm model with spatial constraints for brain mr image segmentation," *Information*, vol. 10, no. 2, p. 74, 2019.

[30] P. Lin, Y. Yang, C.-X. Zheng, and J.-W. Gu, "An efficient automatic framework for segmentation of mri brain image," in *The Fourth International Conference onComputer and Information Technology, 2004. CIT'04.*, vol. 26, pp. 896–900, IEEE, 2004.

[31] P. Lin, Y. Yang, C.-X. Zheng, and J.-W. Gu, "An efficient automatic framework for segmentation of mri brain image," in *The Fourth International Conference onComputer and Information Technology, 2004. CIT'04.*, vol. 22, pp. 896–900, IEEE, 2004.

[32] T. Pavlidis and Y.-T. Liow, "Integrating region growing and edge detection," *IEEE Transactions on Pattern Analysis and Machine Intelligence*, vol. 12, no. 3, pp. 225–233, 1990.

[33] B. Khorram and M. Yazdi, "A new optimized thresholding method using ant colony algorithm for mr brain image segmentation," *Journal of digital imaging*, vol. 32, no. 1, pp. 162–174, 2019.

[34] M. Abd Elaziz, D. Oliva, A. A. Ewees, and S. Xiong, "Multi-level thresholding-based grey scale image segmentation using multi-objective multi-verse optimizer," *Expert Systems with Applications*, vol. 125, pp. 112–129, 2019.

[35] H. Hassannejad, M. S. Pakbaz, and R. Mehdizadeh, "Comparison and evaluation of artificial neural network (ann) training algorithms in predicting soil type classification," *Pharmacology and Life Sciences Bull. Env. Pharmacol. Life Sci*, vol. 4, pp. 212–218, 2015.

[36] T. Awolusi, O. Oke, O. Akinkurolere, A. Sojobi, and O. Aluko, "Performance comparison of neural network training algorithms in the modeling properties of steel fiber reinforced concrete," *Heliyon*, vol. 5, no. 1, p. e01115, 2019.

[37] B. Eren, M. Yaqub, and V. Eyüpoğlu, "Assessment of neural network training algorithms for the prediction of polymeric inclusion membranes efficiency," *Sakarya Üniversitesi Fen Bilimleri Enstitüsü Dergisi*, vol. 20, no. 3, pp. 533–542, 2016.

[38] Y. Song and H. Yan, "Image segmentation techniques overview," in *2017 Asia Modelling Symposium (AMS)*, vol. 9, pp. 103–107, IEEE, 2017.

[39] W. Z. J. Z. P. L. Y. Li, "Study of image segmentation algorithm based on textural features and neural network," vol. 19, no. 1, pp. 300–303, 2010.

[40] M. S. M. Yasmin and S. Mohsin, "Face recognition based on facial features," *Research Journal of Applied Sciences,*, vol. 4, pp. 879–2886, 2012.

[41] M. S. M. Yasmin and S. Mohsin, "Neural networks in medical imaging applications: A survey," *World Applied Sciences Journal*, vol. 22, pp. 85–96, 2013.

[42] X. D. Lijun Zhang, "The research of image segmentation based on improved neural network algorithm," *Journal of Computing and Information Technology*, vol. 5, pp. 395–397, 2010.

[43] S. D. S. A. Ahmed and K. K. Sarma, "Image texture classification using artificial neural network (ann)," *Proceedings of the IEEE*, vol. 54, pp. 1–4, 2011.

[44] S. M. M. Sharif, M. Raza and J. H. Shah, "Microscopic feature extraction method," *Advanced Networking and Applications*, vol. 4, no. 7, pp. 1700–1703, 2013.

[45] M. R. I. Irum and M. Sharif, "Morphological techniques for medical images: A review.," *Research Journal of Applied Sciences*, vol. 4, pp. 2948–29625, 2012.

[46] S. P. N.R. Pal, "A review on image segmentation techniques, pattern recognition," *IEEE Transactions on Medical Imaging*, vol. 26, no. 9, pp. 1277–1294, 1993.

[47] L. C. J.C. Bezdek, L.O. Hall, "Review of mr image segmentation techniques using pattern recognition," *Journal of Computing and Information Technology*, vol. 20, no. 4, pp. 1033–1048, 1993.

[48] S. G. W.E. Blanz, "A connectionist classifier architecture applied to image segmentation," *IEEE Transactions on Medical Imaging*, vol. 12, pp. 272–277, 1990.

[49] P. V. J. S. U. Raff, A.L. Scherzinger, "Quantitation of grey matter, white matter, and cerebrospinal fluid from spin-echo magnetic resonance images using an artificial neural network technique," *Journal of Computing and Information Technology*, vol. 21, no. 12, pp. 1933–1942, 1994.

[50] J. Hopfield, "Neural networks and physical systems with emergent collective computational abilities," *IEEE Transactions on Medical Imaging*, vol. 79, pp. 2554–2558, 1982.

[51] J. Hopfield, "Neurons with graded response have collective computational properties like those of two-state neurons, biophysics," *Journal of Computing and Information Technology*, vol. 81, pp. 3088–3092, 1984.

[52] "Neural" Computation of Decisions in Optimisation Problems, Biol.Cybern., author=J.J. Hopfield, D.W, journal=IEEE Transactions on Medical Imaging, volume=52, pages=141-152, year=1985, publisher=Cambridge Univ Press,"

[53] F. Aysen, Kütahyalıoglu and Karakoç, "Exponential stability of hopfield neural networks with conformable fractional derivative," vol. 456.

[54] Y. T. S.C. Amartur, D. Piraino, "Optimization neural networks for the segmentation of magnetic resonance images," *IEEE Transactions on Medical Imaging*, vol. 11, no. 2, pp. 215–220, 1992.

[55] S. C. G. C. G. Valli, R. Poli, "Neural networks and priori knowledge help the segmentation of medical images," *Journal of Computing and Information Technology*, vol. 2, pp. 117–133, 1998.

[56] C. C. W. Lin, E. Chen-Kuo, "Constraint satisfaction neural networks for image segmentation, pattern recognition," *Journal of Computing and Information Technology*, vol. 25, no. 7, pp. 679–693, 1992.

[57] D. T. D.L. Wang, "Image segmentation based on oscillatory correlation," *IEEE Transactions on Medical Imaging*, vol. 9, pp. 805–836, 1997.

[58] J. G. S. Chakravarthy, V. Ramamurti, "A network of oscillating neurons for image segmentation," *Intelligent Engineering through ANN*, vol. 5, 1995.

[59] R. Y. N. Shareef, D.L. Wang, "Segmentation of medical images using legion," *IEEE Transactions on Medical Imaging*, vol. 18, no. 1, pp. 74–91, 1999.

[60] D. W. X. Liu, "Range image segmentation using a relaxation oscillator network," *IEEE Transactions on Neural Networks*, vol. 19, no. 3, pp. 564–573, 1999.

[61] M.-T. A.Ghaffaria H.Abdollahib M.R.KhoshayandaI. Soltani BozchaloicA.Dadgara, "Performance comparison of neural network training algorithms in modeling of bimodal drug delivery," *International Journal of Pharmaceutics*, vol. 9, pp. 126–138, 2006.

[62] J. K.] S. Haring, M.A. Viergever, "Kohonen networks for multiscale image segmentation, image and vision computing," *Image and Vision Computing,*, vol. 12, no. 6, pp. 339–344, 1994.

[63] R. Tabbussum and A. Q. Dar, "Comparative analysis of neural network training algorithms for the flood forecast modelling of an alluvial himalayan river," *Journal of Flood Risk Management*, vol. 13, no. 4, p. e12656, 2020.

[64] . Mahbuba Begum 1 and M. S. U. 2ORCID1, "Digital image watermarking techniques: A review," *mdpi*, vol. 9, pp. 1–38, 2020.

[65] A. Zeki, A.M.; Manaf, "A novel digital watermarking technique based on isb (intermediate significant bit)," *World Acad. Sci. Eng. Technol. Int. J. Comput. Inf. Eng*, vol. 3, p. 444–451, 2009.

[66] Habes, "Information hiding in bmp image implementation, analysis and evaluation," *Inf. Transm. Comput. Netw*, vol. 11, p. 1–10, 2006.

[67] A. Z. A. Mohammed, G.N.; Yasin, "Robust image watermarking based on dual intermediate significant bit (disb)," in *In Proceedings of the 6th International Conference on CSIT, Amman, Jordan*, vol. 23, p. 444–451, 2014.

[68] D. M. N. L. A. Bender, W.; Gruhl, "Techniques for data hiding," *IBM Syst. J*, vol. 23, p. 313–336, 1996.

[69] R. Singh, P.; Chadha, "A survey of digital watermarking techniques, applications and attacks," *Int. J. Eng. Innov. Technol.*, vol. 2, p. 165–175, 2013.

[70] J. G. Z. H. J. Wu, X.; Hu, "A secure semi-fragile watermarking for image authentication based on integer wavelet transform with parameters," *Inf. Transm. Comput. Netw*, vol. 2, p. 65–75, 2020.

[71] I.-K. Y. . H. J. Kim, "Generalized patchwork algorithm for image watermarking," *Multimedia Systems*, vol. 5, p. 261–265, 2003.

[72] S. Saqib, M.; Naaz, "Spatial and frequency domain digital image watermarking techniques for copyright protection," *Int. J. Eng. Sci. Technol*, vol. 9, p. 691–699, 2017.

[73] L. Z. J. A. A. Tao, H.; Chongmin, "Robust image watermarking theories and techniques: A review," *J. Appl. Res. Technol*, vol. 12, p. 122–138, 2014.

[74] A. Roy, S.; Pal, "A blind dct based color watermarking algorithm for embedding multiple watermarks," *AEU-Int. J. Electron. Commun*, vol. 72, p. 149–161, 2017.

[75] X. A. D. Tsui, T.K.; Zhang, "Color image watermarking using multidimensional fourier transforms," *IEEE Trans. Inf. Forensics Secur*, vol. 3, p. 16–28, 2008.

[76] T. Vaishnavia, D.; Subashini, "Robust and invisible image watermarking in rgb color space using svd.," in *In Proceedings of the International Conference on Information and Communication Technologies, Kochi India,*, vol. 4, p. 1770–1777, 2014.

[77] M. Begum and M. S. Uddin, "Digital image watermarking techniques: A review," *MDPI*, vol. 9, pp. 1–38, 2020.

[78] E. Najafi, "A robust embedding and blind extraction of image watermarking based on discrete wavelet transform," *J. Math. Sci.*, vol. 1, p. 307–318, 2017.

[79] Q. Z. H. Jia, S.; Zhou, "A novel color image watermarking scheme based on dwt and qr decomposition," *J. Appl. Sci. Eng*, vol. 20, p. 193–200, 2017.

[80] S. Shih, F.Y.; Wu, "Combinational image watermarking in the spatial and frequency domains," *J. Pattern Recognit. Soc.*, vol. 36, p. 969–975, 2003.

[81] A. Kumar, "A review on implementation of digital image watermarking using lsb and dwt," *Inf. Commun. Technol. Sustain. Dev*, vol. 22, p. 595–602., 2019.

[82] S. Abdulrahman, A.K.; Ozturk, "A novel hybrid dct and dwt based robust watermarking algorithm for color images.," *Multimed. Tools Appl*, vol. 78, p. 17027–17049, 2019.

[83] A. Savakar, D.G.; Ghuli, "Robust invisible digital image watermarking using hybrid scheme," *Arab. J. Sci. Eng.*, vol. 12, p. 3995–4008, 2019.

[84] S. Voloshynovskiy, "Attacks on digital watermarks: Classification, estimation-based attacks, and benchmarks," *Research Gate*, vol. 8, pp. 118 –126, 2001.

[85] M. M. Chunlin Song, Sud Sudirman and D. Llewellyn-Jones, "Analysis of digital image watermark attacks," *Arab. J. Sci. Eng.*, vol. 3, p. 300–310, 2010.

[86] C.-S. H. . S.-F. Tu, "Enhancing the robustness of image watermarking against cropping attacks with dual watermarks," *Multimedia Tools and Applications*, vol. 6, p. 11297–11323, 2019.

[87] Q. Su, "Novel blind colour image watermarking technique using hessenberg decomposition," *IET Image Process*, vol. 11, p. 817–829, 2016.

[88] Q. Su and B. Chen, "A novel blind color image watermarking using upper hessenberg matrix," *AEU-Int. J. Electron. Commun*, vol. 76, pp. 64–71, 2017.

[89] A. P. I. A. Ansari and C. W. Ahn, "'robust and false positive free watermarking in iwt domain using svd and abc," *Eng. Appl. Artif. Intell*, vol. 49, p. 114–125, 2016.

[90] P. Q. Z. H. Wei and Y. Q. Fu, "Perceptual digital watermark of images using wavelet transform," *IEEE Trans. Consum. Electron*, vol. 44, pp. 1267–1272,, 1998.

[91] O. Jane and E. Elbaşi, "A new approach of nonblind watermarking methods based on dwt and svd via lu decomposition," *Turkish J. Electr. Eng. Comput. Sci*, vol. 22, p. 1354–1366, 2014.

[92] A. S.] A. Mishra, C. Agarwal and P. Bed, "Optimized gray-scale image watermarking using dwt–svd and firefly algorithm," *Expert Syst.Appl*, vol. 41, p. 7858–7867, 2014.

[93] J.-L. L. T.-W. K. R.-S. Run, S.-J. Horng and R.-J. Chen, "An improved svd-based watermarking technique for copyright protection,'," *Expert Syst. Appl*, vol. 39, pp. 673–689, 2012.

[94] R. Shang, B. Ara, I. Zada, S. Nazir, Z. Ullah, and S. U. Khan, "Analysis of simple k-mean and parallel k-mean clustering for software products and organizational performance using education sector dataset," *Scientific Programming*, vol. 2021, pp. 110–121, 2021.

[95] Y. Jeong, J. Lee, J. Moon, J. H. Shin, and W. D. Lu, "K-means data clustering with memristor networks," *Nano letters*, vol. 18, no. 7, pp. 4447–4453, 2018.

[96] T. G. Debelee, F. Schwenker, S. Rahimeto, and D. Yohannes, "Evaluation of modified adaptive k-means segmentation algorithm," *Computational Visual Media*, vol. 5, no. 4, pp. 347–361, 2019.

[97] R. Ahuja, A. Solanki, and A. Nayyar, "Movie recommender system using k-means clustering and k-nearest neighbor," in *2019 9th International Conference on Cloud Computing, Data Science & Engineering (Confluence)*, vol. 20, pp. 263–268, IEEE, 2019.

[98] M. N. Akhtar, W. Ahmed, M. R. Kakar, E. A. Bakar, A. Othman, and M. Bueno, "Implementation of parallel k-means algorithm to estimate adhesion failure in warm mix asphalt," *Advances in Civil Engineering*, vol. 2020, pp. 347–361, 2020.

[99] S. Vyas and A. Prasad, "Analysis of algorithms k-means and apriori for data mining," in *Rising Threats in Expert Applications and Solutions*, vol. 23, pp. 187–191, Springer, 2021.

[100] A. Shukla, S. Kumar, and H. Singh, "Ann based execution time prediction model and assessment of input parameters through ism.," *Int. Arab J. Inf. Technol.*, vol. 17, no. 5, pp. 683–691, 2020.

[101] J. Lian, Z. Yang, J. Liu, W. Sun, L. Zheng, X. Du, Z. Yi, B. Shi, and Y. Ma, "An overview of image segmentation based on pulse-coupled neural network," *Archives of Computational Methods in Engineering*, vol. 28, no. 2, pp. 387–403, 2021.

[102] I. J. H.-Y. L. .-L. C. S. Y. D. W. JUNXIU LIU 1, (Member and R. ZHOU1, "An optimized image watermarking method based on hd and svd in dwt domain," *Arab. J. Sci. Eng.*, vol. 70, pp. 80849–80860, 2019.